Quasi-thermal noise spectroscopy: The art and the practice

N. Meyer-Vernet, K. Issautier, M. Moncuquet

JOURNAL OF GEOPHYSICAL RESEARCH, VOL. 122, DOI:0.1002/2017JA024449

Quasi-thermal noise spectroscopy: the art and the practice[1]

N. Meyer-Vernet,[2] K. Issautier[2], and M. Moncuquet[2]

Corresponding author: N. Meyer-Vernet, LESIA, Observatoire de Paris. (nicole.meyer@obspm.fr)

[1]Dedicated to the memory of Jean-Louis Steinberg

[2]LESIA, Observatoire de Paris, PSL Research University, CNRS, Sorbonne Univ., UPMC, Univ. Paris Diderot, Sorbonne Paris Cité, 92195 Meudon, France

received 8 Jun, 2017, accepted 22 Jul 2017

Key Points.

- ◦ We provide new calculations and analytical approximations for plasma measurements by QTN spectroscopy
- ◦ We study the compatibility with various space implementations and constraints
- ◦ We give some applications for future space missions

Abstract. Quasi-thermal noise spectroscopy is an efficient tool for measuring in situ macroscopic plasma properties in space, using a passive wave receiver at the ports of an electric antenna. This technique was pioneered on spinning spacecraft carrying very long dipole antennas in the interplanetary medium - like ISEE-3 and Ulysses - whose geometry approached a "theoretician's dream". The technique has been extended to other instruments in various types of plasmas onboard different spacecraft and will be implemented on several missions in the near future. Such extensions require different theoretical modelizations, involving magnetized, drifting or dusty plasmas with various particle velocity distributions, and antennas being shorter, biased or made of unequal wires. We give new analytical approximations of the plasma quasi-thermal noise (QTN), and study how the constraints of the real world in space can (or cannot) be compatible with plasma detection by QTN spectroscopy. We consider applications to the missions Wind, Cassini, Bepi-Colombo, Solar Orbiter and Parker Solar Probe.

1. Introduction

Thermal electromagnetic radiation, on which rely a large part of remote observations in astronomy and geophysics, is related to thermal fluctuations in radio-engineering circuits - the so-called Johnson noise - via the fluctuation-dissipation theorem. In the classical approximation, Nyquist's formula [*Nyquist*, 1928] tells us that a wave receiver in open circuit at the ports of an electric antenna immersed in black-body radiation of temperature T measures a voltage power spectrum

$$V_f^2 = 4k_B TR \tag{1}$$

where $hf \ll k_B T$ (h being the Planck constant) and $R = R_{EM}$ is the antenna radiation resistance (Figure 1, left). However most space missions involve electric antennas immersed in plasmas (Figure 1, right), where the quasi-thermal motion of electric charges produces electrostatic fluctuations generally exceeding the radiation electromagnetic field. In that case the main contribution to the measured power is the plasma quasi-thermal noise (QTN, Figure 2). This noise represents the long-wavelength measurement limit in radioastronomy [*Meyer-Vernet et al.*, 2000] and it has been suggested to play a major role in the production of non-thermal electrons in the solar wind ([*Yoon et al.*, 2016] and references therein).

In the ideal case of a plasma at equilibrium temperature T, this noise reduces to Nyquist's formula (1) with $R = R_P$, the antenna resistance resulting from the plasma thermal fluctuations. If the plasma is non-thermal, the noise is still fully determined by the particle velocity distributions provided it is stable [e.g., *Sitenko*, 1967; *Fejer and Kan*, 1969]. This result can be generalized to a magnetized plasma and enables one to deduce the plasma properties from the measured voltage spectrum [*Meyer-Vernet*, 1979]. Since these electrostatic waves are significantly damped by the medium, the measured plasma properties are local ones, so that QTN spectroscopy provides in situ measurements [e.g., *Meyer-Vernet and Perche*, 1989], contrary to the usual spectroscopy based on electromagnetic waves, which provides remote measurements.

This technique was pioneered aboard ISEE-3 which carried the most sensitive radio receiver ever flown [*Knoll et al.*, 1978]. Rather ironically, the paper which pioneered the technique [*Meyer-Vernet*, 1979], submitted ten days before the ISEE-3 launch, was in the process of being rejected on the grounds that the theory was too simple for being applicable in the solar wind, when the data of the inboard radio receiver became available; their agreement with the simple formulas proposed in the submitted manuscript prompted its immediate acceptance. This paper also provided a logically satisfying explanation for several observations previously interpreted as "new" emissions or instabilities, since " *pluralitas non est ponenda sine necessitate"* [*Ockham*, 1324]; the QTN explanation was soon confirmed by *Hoang et al.* [1980] and *Sentman et al.* [1982].

The QTN measurement technique was subsequently used in various environments using radio receivers that had similarly not been designed for that purpose [e.g., *Meyer-Vernet et al.*, 1998]. In particular for measuring on ISEE-3/ICE the electron density and temperature in a comet's tail [*Meyer-Vernet et al.*, 1986a, b], where the electrons were too cold for the inboard particle analyzer to measure them accurately. The QTN technique was also used to measure the solar wind electron properties as a function of heliocentric distance [*Hoang et al.*, 1992] and outside the ecliptic on Ulysses [e.g., *Issautier et al.*, 1998, 1999, 2008; *Le Chat et al.*, 2011], and at 1 AU on WIND [e.g., *Salem et al.*, 2001;

Issautier et al., 2005]. And also in planetary environments such as the Earth's outer plasmasphere [*Lund et al.*, 1994], the Io plasma torus [e.g., *Meyer-Vernet et al.*, 1993; *Moncuquet et al.*, 1995, 1997], and Saturn's magnetosphere [e.g., *Moncuquet et al.*, 2005; *Schippers et al.*, 2013] using the RPWS experiment on Cassini [*Gurnett et al.*, 2004].

Why is the QTN technique so well adapted to measure the electron density and temperature? There are four reasons for that. First of all, both properties are revealed in situ by the location and broad spectral shape of the plasma frequency peak (see Figure 2), just as traditional spectroscopy reveals the chemical composition and the temperature (albeit remotely). Second, being passive, this instrument does not perturb the medium, contrary to other wave techniques. Third, since it is based on electrostatic waves or fluctuations of wavelength of the order or greater than the Debye length (or the electron gyroradius if the plasma is strongly magnetised) and tending to infinity close to resonances, the technique is equivalent to a detector of cross-section larger by several orders of magnitude than that of classical detectors. And finally, for the same reason, it is relatively immune to spacecraft photoelectrons and charging effects which affect traditional particle analyzers; in particular, since the electron density is deduced from a spectral peak, this measurement is independent on gain calibrations. Because of its reliability and accuracy, QTN spectroscopy serves routinely to calibrate other instruments [e.g., *Maksimovic et al.*, 1995; *Issautier et al.*, 2001; *Salem et al.*, 2001].

The drawback is that, contrary to the classical particle analysers, QTN spectroscopy cannot measure directly the particle velocity distributions. Even though some moments are revealed by spectral features (see Section 2), a full measurement requires solving an inverse problem: modelise the electric antenna and the velocity distribution(s) with a few parameters, calculate the corresponding QTN spectrum, and fitting the theory to the data to determine the parameters of the distribution as sketched in Figure 2. In other words, the QTN technique has the cons and pros of a global measurement: it measures less parameters, but it can measure them faster and more accurately. Note, too, that the technique is less adapted to measure the ions because they are revealed at lower frequencies (Section 2.8) at which the spectrum can be spoiled by the shot noise.

This shot noise, produced by the fluctuations due to collection and emission of individual electric charges by the antenna surface, can be a real nuisance for QTN spectroscopy. It is very hard to modelize because, contrary to the QTN, it depends on the antenna floating potential, which is badly known because the photoelectron and secondary emissions of materials in space change significantly with ageing and have different properties from those measured in the laboratory [e.g., *Kawasaki et al.*, 2016]. This shot noise is generally negligible for wire dipole antennas around f_p [*Meyer-Vernet and Perche*, 1989], but this is not so when the antennas are made of small spheres. Indeed, the shot noise is proportional to the squared voltage produced by each charge collected or emitted ($\propto a^{-2}$ for spheres of radius a since their capacitance $\propto a$), and to the events' rate - proportional to surface area ($\propto a^2$), so that the variation with a cancels out. Therefore, the shot noise on spheres does not decrease as their radius decreases, contrary to wires whose surface $\propto a$ whereas the capacitance varies weakly with radius. This is the basic reason why spherical probes are unadaptated for QTN spectroscopy, in addition to the fact that these probes must be supported by difficult-to-modelize booms. For all these reasons, we will only consider wire antennas in this paper, and will mention the shot noise only for estimating the extent to which it may spoil QTN spectroscopy, in particular for fat or biased antennas (see Section 3.2).

Simple analytical approximations are invaluable for the preliminary design and interpretation of space experiments. A number of such approximations were derived when QTN spectroscopy was not yet a recognized technique and was used as a by-product of radioastronomy experiments [*Meyer-Vernet and Perche*, 1989]. This technique will now be implemented in the inner heliosphere by Solar Orbiter with shorter antennas [*Maksimovic et al.*, 2005; *Zouganelis et al.*, 2007], and with specifically designed instruments in Mercury's environment by Bepi-Colombo [*Moncuquet et al.*, 2006a] and in the solar corona with Parker Solar Probe (PSP) [*Bale et al.*, 2016]. The properties of the wire dipole antennas used in these missions are summarized in Table 1, together with those of some previous missions; we do not include STEREO, whose antennas' length is too short for implementing QTN spectroscopy except in very high density structures [*Zouganelis et al.*, 2010] (see Section 2.4).

This paper is organized as follows. Section 2 recalls the main properties of QTN under different conditions and gives new analytical approximations having a wide range of applications, in particular for antennas of moderate length in non-thermal plasmas. Section 3 extends the calculations made for ideal cases (Figure 3) to antennas being unsymmetrical or biased and to dusty plasmas. Unless otherwise stated, units are SI.

2. The Art

The basic shape of the QTN spectrum can be understood from simple plasma physics [*Meyer-Vernet and Perche*, 1989]. Each charged particle passing by the antenna induces a voltage pulse. This voltage is not Coulomb-like because the plasma particles are "dressed" by their mutual coupling. At time scales corresponding to frequencies $f < f_p$, this dressing takes the simple form of a Debye sheath of scale L_D, the Debye length, so that each thermal electron produces on the antenna a voltage pulse of duration roughly equal to the time that it remains within a Debye length, i.e. about $1/(2\pi f_p)$; the Fourier transform of such a pulse is a constant for $f < f_p$, producing a plateau of amplitude determined by the bulk of the electrons. In contrast at higher frequencies, moving electrons excite plasma waves so that their dresses become more sophisticated [e.g., *Meyer-Vernet*, 1993], trailing long trains of Langmuir waves which produce the plasma frequency peak.

2.1. Basics

In the Vlasov framework, the plasma can be thought of as an assembly of independent test particles "dressed" by their collective interactions which determine the plasma dielectric permittivity defining the plasma spatial and temporal dispersion [*Rostoker*, 1961]. In the electrostatic limit ($\omega/kc \ll 1$, where $\omega = 2\pi f$ is the angular frequency, $\mathbf{k}$ the wave vector and c the speed of light), the (linear) longitudinal ($\mathbf{E} \parallel \mathbf{k}$) electric field fluctuations in Fourier space are given from Poisson's equation by [*Sitenko*, 1967]

$$\langle E^2(\mathbf{k}, \omega)\rangle = \frac{\langle \rho^2(\mathbf{k}, \omega)\rangle^{(0)}}{k^2\epsilon_0^2|\epsilon_L(\mathbf{k}, \omega)|^2} \tag{2}$$

where $\epsilon_L(\mathbf{k}, \omega)$ is the longitudinal dielectric function and $\langle \rho^2(\mathbf{k}, \omega)\rangle^{(0)}$ the free-space (test-particle) charge density fluctuations (in Fourier space) produced by quasi-thermal particle motions. In a weakly magnetized plasma ($\omega \gg \omega_g$, the electron angular gyrofrequency), the test particles can be assumed to move in straight lines, so that with a velocity distribution $f(\mathbf{v})$

$$\langle \rho^2(\mathbf{k},\omega)\rangle^{(0)} = 2\pi e^2 \int d^3v f(\mathbf{v})\delta(\omega - \mathbf{k}.\mathbf{v}) \tag{3}$$

the particle number density being

$$n = \int d^3v f(\mathbf{v}) \tag{4}$$

In the presence of a magnetic field $\mathbf{B}$, the test particles follow helical orbits of (angular) gyrofrequency ω_g, so that

$$\langle \rho^2(\mathbf{k},\omega)\rangle^{(0)} = 2\pi e^2 \sum_{-\infty}^{\infty} \int d^3v f(\mathbf{v}) J_n^2(k_\perp v_\perp/\omega_g)\ \delta(\omega - n\omega_g - k_\parallel v_\parallel) \tag{5}$$

where $v_\parallel$ and $v_\perp$ are the velocity components respectively parallel and perpendicular to $\mathbf{B}$ and J_n are n^{th} order Bessel functions of the first kind [*Abramowitz and Stegun*, 1965].

With an electric antenna characterized by the current distribution $\mathbf{J}(\mathbf{k})$ in Fourier space, immersed in a plasma drifting with velocity $\mathbf{V}$, the voltage power at the antenna ports at frequency f is

$$V_f^2 = \frac{2}{(2\pi)^3} \int d^3k\ \frac{|\mathbf{k}.\mathbf{J}|^2}{k^2}\ \langle E^2(\mathbf{k},\omega - \mathbf{k}.\mathbf{V})\rangle \tag{6}$$

The power V_r^2 at the ports of a receiver of impedance Z_r is deduced from

$$V_r^2/V_f^2 = |Z_r/(Z_r + Z_a)^2| \tag{7}$$

where Z_a is the antenna impedance.

2.2. Electric Antenna Response

For the simplest antenna, made of two aligned wires, each of length $L \ll \lambda$ and radius $a \ll [L_D, L]$ (Figure 1), the current distribution can be assumed to be triangular [*Meyer and Vernet*, 1974], so that

$$|\mathbf{k}.\mathbf{J}| = |\frac{4\sin^2(k_\parallel L/2)}{k_\parallel L} J_0(k_\perp a)| \tag{8}$$

where $k_\parallel$ and $k_\perp$ are the $\mathbf{k}$ components respectively parallel and perpendicular to the antenna direction (see details in [*Schiff*, 1970; *Couturier et al.*, 1981]). In most cases of interest, the wave numbers responsible for the noise are smaller than or of the order of the plasma Debye length (or the electron gyroradius if it is smaller), with $ka \ll 1$, so that $J_0(k_\perp a) \simeq 1$ except in very dense and cold plasmas as planetary ionospheres. An important consequence emerges from (8). Writing $k_\parallel L = kL\cos\alpha$ where α is the angle between $\mathbf{k}$ and the antenna direction, one sees that whereas a short antenna ($kL \ll 1$) is mainly sensitive to $\mathbf{k}$ parallel to the antenna ($\cos\alpha = 1$) as for electromagnetic waves, on the contrary a long antenna ($kL \gg 1$) is mainly sensitive to wave vectors roughly perpendicular to its proper direction [*Meyer-Vernet*, 1994].

If the plasma fluctuations are isotropic in the antenna frame (which holds with $V = 0$ and an isotropic velocity distribution in a weakly magnetized plasma), (6) becomes

$$V_f^2 = \frac{8}{\pi^2}\int_0^\infty dk\; F(kL)\langle E^2(k,\omega)\rangle \tag{9}$$

with

$$F(x) = 1/(32\pi) \int d\Omega \, |\mathbf{k}.\mathbf{J}|^2 = [\mathrm{Si}(x) - \mathrm{Si}(2x)/2 - 2\sin^4(x/2)/x] J_0^2(xa/L)/x \tag{10}$$

where Si(x) $= \int_0^x dt \ \sin t/t$ is the sine integral function [*Abramowitz and Stegun*, 1965]. Two approximations are useful:

$$F(x) \simeq x^2/24 \quad \text{for} \ \ x < 1 \tag{11}$$

$$F(x) \simeq \pi/(4x) \quad \text{for} \ \ x \gg 1 \tag{12}$$

with (11) approximating (10) better than 5% when $x \lesssim 1$.

When the plasma fluctuations are anisotropic with a symmetry axis (for example with a drift of velocity $\mathbf{V}$ or a static magnetic field $\mathbf{B}$), a different simplification arises. Since in that case the electric fluctuations are independent of the azimuthal angle ϕ around the symmetry axis, (6) can be calculated as

$$V_f^2 = \frac{1}{2\pi^2} \int_0^\infty dk \int_0^\pi \sin\theta \, d\theta \, \langle E^2(k, \theta, \omega - k.V\cos\theta) \rangle \int_0^{2\pi} \frac{d\phi}{2\pi} \, |\mathbf{k}.\mathbf{J}|^2 \tag{13}$$

where θ is the angle between $\mathbf{k}$ and the symmetry axis and (8) yields

$$\int_0^{2\pi} \frac{d\phi}{2\pi} \, |\mathbf{k}.\mathbf{J}|^2 = \frac{8}{\pi} \int_0^{2\pi} d\phi \, \frac{\sin^4(kL\cos\alpha/2)}{(kL\cos\alpha)^2} J_0^2(ka\sin\alpha) \tag{14}$$

α being the angle between $\mathbf{k}$ and the antenna direction, given by

$$\cos\alpha = \cos\theta\cos\beta + \sin\theta\sin\beta\cos\phi \tag{15}$$

where β is the angle between the antenna and the symmetry axis.

If the antenna is parallel to the symmetry axis ($\beta = 0$), the QTN is given by (13) with from (8)

$$\int_0^{2\pi} \frac{d\phi}{2\pi} \, |\mathbf{k}.\mathbf{J}|^2 = \left[\frac{4\sin^2(kL\cos\theta/2)}{|kL\cos\theta|} J_0(ka\sin\theta) \right]^2 \tag{16}$$

On the other hand, if the antenna is perpendicular to the symmetry axis ($\beta = \pi/2$), (15) reduces to $\cos\alpha = \sin\theta\cos\phi$, so that with the change of variable $s = kL\sin\theta\cos\phi$ in the integral (14), we find

$$\int_0^{2\pi} \frac{d\phi}{2\pi} \, |\mathbf{k}.\mathbf{J}|^2 = F_\perp(kL\sin\theta)/2 \tag{17}$$

$$F_\perp(x) = \frac{64}{\pi} \int_0^x ds \frac{\sin^4(s/2)}{s^2(x^2 - s^2)^{1/2}} \tag{18}$$

$$= \frac{8}{x}[2\int_0^x dt J_0(t) - \int_0^{2x} dt J_0(t) + J_1(2x) - 2J_1(x)] \tag{19}$$

where we have assumed $ka \ll 1$. Equation (19) yields $F_\perp(x) \simeq x^2$ for $x < 1$, and $F_\perp(x) \simeq 8/x$ for $x \gg 1$.

The antenna response $F_\perp(x)$, given by (18)-(19) with $x = kL\sin\theta\sin\beta$, is also relevant whatever the antenna direction in a particular case: **k** roughly perpendicular to the symmetry axis. Therefore the function $F_\perp$ was used both for calculating the quasi-thermal noise in Bernstein waves [*Meyer-Vernet et al.*, 1993; *Moncuquet et al.*, 1995] (see Section 2.4) and the Doppler-shifted quasi-thermal noise of ions [*Issautier et al.*, 1999] (see Section 2.8).

2.3. Dealing with Non-Maxwellians: Generalized Temperatures

Non-maxwellian velocity distributions are ubiquitous in space plasmas. The culprits are Coulomb collisions, whose cross-section decreases as the inverse square of the particle energy, so that, even when the bulk of the distribution is dominated by collisions, the faster particles are not, making suprathermal tails ubiquitous [e.g., *Scudder and Olbert*, 1979; *Scudder and Karimabadi*, 2013]. Contrary to Maxwellians which are completely defined by two parameters (density and temperature), non-thermal distributions raise a major problem for measuring devices because their full characterization may need an infinite number of parameters. Indeed, sixty years after the beginning of the space age, nobody knows the accurate shape of particle velocity distributions in space. This is especially true for electrons, which either cannot be detected at energies (in eV) smaller than the absolute value of the spacecraft potential if it is negative - as occurs in inner planetary magnetospheres, or are strongly perturbed by this potential and by photoelectrons if it is positive - as occurs in the solar wind [e.g., *Garrett*, 1981; *Whipple*, 1981].

Still worse, in the absence of equilibrium, the "temperature" revealed by instruments generally depends on the measured energy range. In order to derive generic results, it is useful to characterize an isotropic non-maxwellian velocity distribution, depending on the speed v, by its generalized temperatures defined as [*Meyer-Vernet*, 2001]

$$k_B T_q/m = (\langle v^q \rangle / c_q)^{2/q} \tag{20}$$

$$c_q = (q+1)!! \qquad \text{for } q \text{ even} \tag{21}$$

$$c_q = \frac{2^{1+q/2}}{\pi^{1/2}} \left(\frac{q+1}{2} \right)! \quad \text{for } q \text{ odd} \tag{22}$$

where $q > -3$ is an integer, m is the electron mass, k_B is Boltzmann's constant, and the scalar moment of order q is

$$\langle v^q \rangle = \int d^3v \, v^q f(\mathbf{v})/n \tag{23}$$

The coefficients c_q are defined so that if the distribution is Maxwellian, all T_q's are equal to its classical temperature. The smaller the index q, the slower the particles responsible for T_q, and for velocity distributions having a suprathermal tail, the smaller the value of T_q. In particular

$$T_2 = m\langle v^2 \rangle/(3k_B) \equiv T \tag{24}$$

is the classical kinetic temperature, T_1 is related to the mean random speed $\langle v \rangle$ as

$$\langle v \rangle = [8k_B T_1/(\pi m)]^{1/2} \tag{25}$$

and T_{-2} is related to the Debye length L_D as

$$L_D = [\epsilon_0 k_B T_{-2}/(ne^2)]^{1/2} \tag{26}$$

Therefore an instrument detecting essentially the low-energy particles (which determine the Debye length), will find, if a Maxwellian is assumed, a temperature close to T_{-2}, whereas an instrument measuring the flux will find a temperature close to T_1. It is therefore not surprising that a number of temperature measurements in which a Maxwellian is assumed are inconsistent, so that new methods are being devised ([e.g., *Dudík et al.*, 2017] and references therein).

The simplest way of representing a distribution having a supra-thermal tail is the so-called kappa distribution [*Vasyliunas*, 1968], which can be written

$$f_\kappa(v) \propto [1 + v^2/(\kappa v_0^2)]^{-(\kappa+1)} \tag{27}$$

and has been used for modelling the QTN by *Chateau and Meyer-Vernet* [1991]; *Zouganelis et al.* [2008]; *Le Chat et al.* [2009]. Since the probability for the speed to lie in the range $[v, v + dv]$ is $f_\kappa(v) \times 4\pi v^2 dv$ and we have $\left[\frac{d}{dv}[v^2 f_\kappa(v)]\right]_{v=v_0} = 0$, the most probable speed equals v_0. The greater the value of κ, the closer is the distribution to a Maxwellian, with $f_\kappa(v) \to e^{-v^2/v_0^2}$ when $\kappa \to \infty$.

At low speeds, developing (27) in series yields $f_\kappa(v) \propto 1 - (1 + 1/\kappa)v^2/v_0^2$; hence the Kappa distribution decreases faster with v than the Maxwellian $e^{-v^2/v_0^2} \propto 1 - v^2/v_0^2$. In contrast, at high speeds $f_\kappa(v) \propto (v^2/\kappa v_0^2)^{-(\kappa+1)}$; hence the Kappa distribution decreases slower than a Maxwellian. This illustrates an interesting property of Kappa distributions. Whereas at low speeds, a Kappa can be fitted by a Maxwellian of temperature smaller than its actual kinetic temperature, its high speed power-law decrease can mimic (albeit in a narrow energy range) a Maxwellian of much higher temperature. Taking these two faces into account can resolve a number of apparent contradictions arising when observations are interpreted with tools that assume Maxwellian distributions [e.g., *Nicholls et al.*, 2012].

With a Kappa distribution (27), we find from (20)

$$T_2 = (mv_0^2/2k_B)\kappa/(\kappa - 3/2) \equiv T \tag{28}$$

$$T_1 = T \times (\kappa - 3/2)\,[\Gamma(\kappa - 1)/\Gamma(\kappa - 1/2)]^2 \tag{29}$$

$$T_{-1} = T \times (\kappa - 3/2)\,[\Gamma(\kappa - 1/2)/\Gamma(\kappa)]^2 \tag{30}$$

$$T_{-2} = T \times (\kappa - 3/2)/(\kappa - 1/2) \tag{31}$$

For example with $\kappa = 4$, we have $T_{-1} \simeq 0.77 \times T$ and $T_{-2} \simeq 0.71 \times T$. From (28), a finite value of the kinetic energy requires $\kappa > 3/2$. On the other hand, the Debye length is given by (26), (28), and (31) as [*Chateau and Meyer-Vernet*, 1991]

$$L_D = \frac{v_0}{\omega_p} \left[\frac{\kappa}{2\kappa - 1} \right]^{1/2} \tag{32}$$

suggesting that the Debye screening has a normal behavior even when κ approaches 3/2, despite some arguments to the contrary [e.g., *Fahr and Heyl*, 2016].

Another popular representation of non-thermal distributions is the sum of a cold ("core") and a hot maxwellian of respective density and temperature n_c, n_h, T_c, T_h, which has one more free parameter than the Kappa distribution. In that case we have $T \equiv T_2 = (n_c T_c + n_h T_h)/(n_c + n_h)$, whereas $T_{-1} = T_c (n_c + n_h)^2 / [n_c + n_h (T_c/T_h)^{1/2}]^2$ and $T_{-2} = (n_c + n_h)/(n_c/T_c + n_h/T_h)$; hence with a dilute hot maxwellian ($n_h/n_c \ll 1$, $T_h/T_c \gg 1$), we have $T_{-1} \simeq T_{-2} \simeq T_c$, the core temperature.

A further popular representation is the sum of a cold Maxwellian (of temperature T_c) containing the bulk of the distribution plus a hot Kappa distribution. Indeed, low-energy particles are generally collisional whereas faster ones are not, and many processes - including the spontaneously emitted Langmuir waves, i.e. the QTN [e.g., *Yoon*, 2014; *Yoon et al.*, 2016] - tend to generate Kappa distributions via non-linearities. In that case, we have as previously $T_{-1} \simeq T_{-2} \simeq T_c$.

2.4. Core Electron Temperature

As noted above, in a weakly magnetized plasma, the electron QTN spectrum exhibits a generic low-frequency plateau which is produced by electrons passing-by the antenna. This suggests that the plateau will mainly reveal the temperature defining the Debye length.

We derive below a generic expression of this plateau, relevant for a number of space radio instruments and independent of the detailed shape of the distribution, provided it is isotropic.

In a weakly magnetized plasma with an isotropic electron velocity distribution, (3) reduces to

$$\langle \rho^2(\mathbf{k},\omega)\rangle^{(0)} = \frac{(2\pi e)^2}{k}\int_{\omega/k}^{\infty} dv\ v\ f(v) \tag{33}$$

which yields for $\omega/kv \ll 1$

$$\langle \rho^2(\mathbf{k},\omega)\rangle^{(0)} \simeq \frac{\pi e^2}{k} n\ \langle v^{-1}\rangle \tag{34}$$

In the same limit, we have

$$\epsilon_L \simeq 1 + \omega_p^2\ \langle v^{-2}\rangle/k^2 \equiv 1 + 1/(k^2 L_D^2) \tag{35}$$

with L_D given by (26). For a wire antenna (Figure 1), Eqs.(2), (9), (34) and (35) yield

$$V_f^2 \simeq \left(\frac{2^7 m k_B\ T_{-2}^2}{\pi^3\epsilon_0^2\ T_{-1}}\right)^{1/2} F_0(L/L_D) \tag{36}$$

$$F_0(t) = \int_0^{\infty} dy\ \frac{y\ F(yt)}{(1+y^2)^2} \tag{37}$$

$F(x)$ being given by (10). The function $F_0(L/L_D)$ is shown in Figure 4. The simple expression (36) of the plateau level is generic since it holds whatever the ratio L/L_D and the shape of the (isotropic) electron velocity distribution.

For $L/L_D \gg 1$, $F(x)$ can be approximated by (12), so that (37) yields

$$F_0(L/L_D) \simeq (\pi^2/16) L_D/L \quad \text{for}\ \ L/L_D \gg 1 \tag{38}$$

whence from (36)

$$V_f^2 \simeq \frac{(\pi/2)^{1/2}}{\epsilon_0 \omega_p L} \frac{k_B\, T_{-2}^{3/2}}{T_{-1}^{1/2}} \simeq \frac{3.5\times 10^{-14}}{n^{1/2} L} \frac{T_{-2}^{3/2}}{T_{-1}^{1/2}} \quad \text{for } \; L/L_D \gg 1 \tag{39}$$

equivalent to a result by *Chateau and Meyer-Vernet* [1991]. One sees on Figure 4 that the approximation (38) (dashed red line), yielding (39), only holds for extremely long antennas. In practice, however, one expects $L/L_D \sim 2.5-6$ for Bepi-Colombo and $L/L_D \sim 1-2.5$ for Solar Orbiter in the solar wind at 0.3 AU,, whereas for Parker Solar Probe at 10 solar radii we have $L/L_D \sim 2-3$.

In these cases, a much better approximation can be derived. Indeed, for $2 \lesssim L/L_D \lesssim 7$, (37) yields $F_0 \simeq 0.05$ within 10% (solid red line in Figure 4),which yields

$$V_f^2 \simeq \frac{1}{\pi^2 \epsilon_0} \left[\frac{m k_B\, T_{-2}^2}{T_{-1}}\right]^{1/2} \simeq 4.07\times 10^{-17} \frac{T_{-2}}{T_{-1}^{1/2}} \quad \text{for } \; 2 \lesssim L/L_D \lesssim 7 \tag{40}$$

With a roughly maxwellian core of temperature T_c and a dilute halo, we have $T_{-2}/T_{-1}^{1/2} \simeq T_c^{1/2}$, whence

$$V_f^2 \simeq 4.07\times 10^{-17} T_c^{1/2} \quad \text{for } \; 2 \lesssim L/L_D \lesssim 7 \tag{41}$$

Note that with a Kappa distribution we have

$$\frac{T_{-2}}{T_{-1}^{1/2}} = T^{1/2}\, \frac{(\kappa - 3/2)^{1/2}\, \Gamma(\kappa)}{\Gamma(\kappa + 1/2)} \tag{42}$$

yielding $T_{-2}^2/T_{-1} \simeq 0.66\times T \simeq 0.93\times T_{-2}$ for $\kappa = 4$, so that the temperature measured via the plateau level is close to that defining the Debye length, similar to a "core" temperature. However with $\kappa = 2$, we have $T_{-2}^2/T_{-1} \simeq 0.85\times T_{-2}$, so that in that case, the plateau yields a temperature smaller than the "core" temperature T_{-2} by about 15%; this reflects the shortage of low-energy particles for kappa distributions with respect to Maxwellians.

Figure 5 shows the levels of the quasi-thermal plateau in a density-core-temperature plane with a dipole antenna made of two colinear $L = 2$ m wires, for applications to Parker Solar Probe/FIELDS. The orange crosses sketch the parameters expected at perihelion ($n \simeq 7000$ cm^{-3}, $T \simeq 10^6$ K). We show the power at both the antenna ports, V_f^2, given by (36) (left) and at the receiver ports, V_r^2, (right). The temperature shown on the vertical axis is T_{-2}^2/T_{-1}, very close to that of the cold Maxwellian when the distribution is a cold Maxwellian with a suprathermal tail. We have superimposed the approximation (40) as red bars. In the low frequency range of the plateau, the dipole antenna impedance reduces to a capacitance [*Meyer-Vernet and Perche*, 1989]

$$C_a \simeq \pi \epsilon_0 L / \ln(L_D/a) \tag{43}$$

when $L/L_D \gg 1$, so that one deduces from (7)

$$V_r^2/V_f^2 \simeq 1/(1 + C_b/C_a)^2 \tag{44}$$

where C_b is the (dipole) load/stray capacitance, which lumps together the receiver input capacity and that of the antenna erecting mechanism, including the capacity between the antenna and the spacecraft structure (the so-called base capacity). With $L = 2$ m, $a = 1.6 \times 10^{-3}$ m and $L_D \simeq 0.8$ m at 10 solar radii, we have $C_a \simeq 8.9$ pF, whence with $C_b = 35$ pF (see Table 1), $V_r^2/V_f^2 \simeq 0.04$. This yields a plateau level at the receiver ports $V_r^2 \simeq 1.7 \times 10^{-15}$ V^{2}Hz^{-1}, which requires a receiver sensitivity of at least a few tens nV Hz$^{-1/2}$. These evaluations assume that the ion (Section 2.8) and shot noise contributions are small enough, which holds in this case, except possibly if the antennas are biased (see Section 3.2).

One sees on Figures 4 and 5 that for smaller values of L/L_D, the plateau level becomes much less sensitive to the temperature; in particular for $L/L_D \simeq 1$, F_0 is nearly proportional to L/L_D, so that the plateau becomes nearly independent of the temperature and cannot be used to measure it; for still smaller lengths, the weak dependence makes the measurement dificult, as is the case for STEREO ($L = 6$ m) at 1 AU.

A very interesting property is that these results also hold in a magnetized plasma if the frequency is a gyroharmonic. Indeed, in that case, as suggested by *Meyer-Vernet et al.* [1993], the magnetic field does not change the QTN level at low frequencies. This can be proven as follows. For $\omega = n\omega_g$, one can factorize in (5) the term $\sum_{-\infty}^{\infty} J_n^2(k_\perp v_\perp/\omega_g)$ (which is equal to unity [*Abramowitz and Stegun*, 1965]). Therefore, $\langle \rho^2(\mathbf{k}, n\omega_g)\rangle^{(0)}$ reduces to the value of $\langle \rho^2(\mathbf{k}, 0)\rangle^{(0)}$ in the absence of magnetic field, which is given by (34). Consider now the dielectric function. In a low-β plasma where transverse and longitudinal modes decouple, we can use (2) in the electrostatic limit, and in the expression of the longitudinal permittivity (e.g. [*Alexandrov et al.*, 1984]) one can similarly factorize $\sum_{-\infty}^{\infty} J_n^2(k_\perp v_\perp/\omega_g) = 1$ when $\omega = n\omega_g$, so that ϵ_L reduces to the low-frequency limit of its unmagnetized value.

This is illustrated in Figure 6, which shows two examples of QTN spectra measured respectively by Wind/Waves in the Earth's magnetosphere, and by Cassini/RPWS in Saturn's magnetosphere. One can see that the "plateau" is in these cases the level at the gyroharmonics (except at the lowest frequencies, for which the shot noise and other contributions are not negligible). Note that, since Cassini/RPWS antennas wires are not collinear - making an angle of 120° - with a significant gap between them [*Gurnett et al.*, 2004], the antenna response should be changed accordingly [*Schippers et al.*, 2013], using the formulas given in [*Meyer-Vernet and Perche*, 1989].

As shown by *Meyer-Vernet et al.* [1993], the frequencies of these minima can be used to measure accurately the modulus of the magnetic field, whereas the increased level between gyroharmonics, produced by the QTN in Bernstein waves (having $\mathbf{k}$ nearly normal to $\mathbf{B}$) - essentially determined by suprathermal electrons [*Sentman et al.*, 1982] - can be used to estimate their energy. The spectra shown in Figure 6 are rather similar to those calculated by *Yoon et al.* [2017] for $\mathbf{k}$ nearly perpendicular to $\mathbf{B}$ (with an integration over k). Note that these calculations are somewhat different from the estimates by *Meyer-Vernet et al.* [1993] who include the response of the antenna, so that they find the QTN between gyroharmonics to be roughly proportional to the temperature of hot electrons and to $F_\perp(kL\sin\theta)$ (θ is the angle between the antenna and $\mathbf{B}$, k corresponds to Bernstein waves and $F_\perp$ is given by (18)-(19)). The factor $F_\perp$ illustrates the interesting counter-intuitive property mentioned in Section 2.2 that a long antenna (with respect to $1/k$) is mainly sensitive to electrostatic waves having $\mathbf{k}$ roughly perpendicular to its proper direction, so that it can receive a large QTN in Bernstein waves when it is oriented relatively close to the magnetic field direction. These calculations have been used to measure the hot electron energy (from the observed power) as well as k (from the modulation with the antenna spin angle) in the Io torus [*Moncuquet et al.*, 1995] and in Saturn's inner magnetosphere [*Moncuquet et al.*, 2005, 2006b].

2.5. Electron Total Density and Kinetic temperature

The most basic properties of a particle velocity distribution are the total electron density and kinetic temperature. In general, these properties are obtained by fitting the QTN spectrum to the data, except in the ideal case of an antenna much longer than the Debye length immersed in an isotropic plasma, for which these properties are revealed without any fitting (Figure 2). Indeed, the QTN spectral peak reveals the plasma frequency - whence the electron density, and at frequencies $f \gg f_p$ we have $\epsilon_L \simeq 1$, so that (2), (9) and (33) yield

$$V_f^2 \simeq \frac{32 m\omega_p^2}{4\pi\epsilon_0} \int_0^{\infty} dv v f(v) \int_{\omega/v}^{\infty} dk F(k)/k^3 \qquad \text{for } \ f \gg f_p \tag{45}$$

If $fL/(f_p L_D) \gg 1$, substituting $F(k) \simeq \pi/(4kL)$ in (45) yields

$$V_f^2 \simeq f_p^2 \; k_B T/(\pi\epsilon_0 L f^3) \tag{46}$$

The high-frequency QTN is directly proportional to the kinetic temperature $T \equiv T_2$ whatever the shape of the velocity distribution. This f^{-3} spectrum is clearly seen on Figure 2. Note that V_f^2 is deduced from the power measured V_r^2 at the receiver ports by using (44) with the dipole antenna capacitance in this high frequency range

$$C_a \simeq \pi\epsilon_0 L/[\ln(L/a) - 1] \tag{47}$$

Such an observation, however, requires that no radioemission perturbs the spectrum. This can be seen on Figure 7 which shows a radio spectrogram from WIND/WAVES acquired in the solar wind during the detection of intense solar radioemissions. The power density below f_p (revealed by the line of increased power), produced by the plasma QTN, remains unperturbed and can still be used to deduce the cold electron temperature (see Section 2.4), but the power is strongly perturbed above f_p and cannot be used for measuring the kinetic temperature.

The total electron density can be deduced from the location of the plasma frequency peak. However, this peak can be shifted from f_p by several effects. First of all, even in the absence of Doppler-shifts, the spectral peak may be slightly shifted from f_p, by an amount which depends on the antenna length (via the factor $F(k)$ in (9) as shown by *Meyer-Vernet and Perche* [1989]), on the distribution of hot electrons and on the frequency and time resolution, as shown in the following section.

2.6. Hot Electrons

Since electrons interact with waves of phase speed equal to their proper speed, and the phase speed of Langmuir waves $\omega/k \rightarrow \infty$ when $\omega \rightarrow \omega_p$, the shape of the plasma frequency peak is determined by high speed electrons; the closer the frequency to f_p, the higher the speed of electrons producing the power. This property is illustrated by the extreme behaviour of the "square" velocity distribution $f(v) \propto \mathrm{H}(v_0 - v)$, the Heaviside step function, which produces no QTN peak at f_p because of the lack of electrons having the proper speed to interact with the waves [*Chateau and Meyer-Vernet*, 1989].

Detecting very high energy electrons via QTN spectroscopy therefore requires two receiver properties which may be difficult to conciliate: a high frequency resolution (to measure accurately the peak shape), and a high temporal resolution (because the spacecraft/plasma relative motion and the turbulence make the electron density near the antenna, whence f_p, change rapidly with time).

To illustrate this point, consider an electron velocity distribution made of a sum of isotropic distributions f_i. From (33), we have

$$\langle \rho^2(\mathbf{k},\omega)\rangle^{(0)} = \frac{(2\pi e)^2}{k}\sum_i B_i(k) \tag{48}$$

where

$$B_i(k) = \int_{\omega/k}^{\infty} dv\ v\ f_i(v) \tag{49}$$

The imaginary part of the longitudinal dielectic function $\epsilon_L(k,\omega)$ is then

$$\mathrm{Im}(\epsilon_L) = \frac{2\pi^2 e^2\omega}{\epsilon_0 m k^3}\sum_i f_i(\omega/k) \equiv I_L \tag{50}$$

For $\omega/kv \gg 1$, the real part of ϵ_L can be approximated by

$$\mathrm{Re}(\epsilon_L) \simeq 1 - (\omega_p^2/\omega^2)\left(1 + k^2\langle v^2\rangle/\omega^2\right) \equiv R_L \tag{51}$$

whose nearly real zero is

$$k_L \simeq \omega\left(\omega^2/\omega_p^2 - 1\right)^{1/2} / \left(\langle v^2\rangle\right)^{1/2} \tag{52}$$

The contribution of this zero to the integral (9) (using (2)) can be calculated by writing $R_L \simeq (k - k_L)\partial R_L/\partial k$ for $k \simeq k_L$ at $f \simeq f_p$, with from (51)

$$\partial R_L/\partial k \simeq -2k_L\langle v^2\rangle/\omega_p^2 \equiv -R_L' \tag{53}$$

Therefore (2) and (9) yield for $f = f_p + \Delta f$ with $\Delta f \ll f_p$

$$V_f^2 \simeq \frac{8}{\pi\epsilon_0^2}\frac{F(k_L L)}{k_L^2}\frac{\langle\rho^2(k_L,\omega_p)\rangle^{(0)}}{R_L'(k_L,\omega_p)I_L(k_L,\omega_p)} \tag{54}$$

Substituting (48), (50) and (53) yields the shape of the QTN peak

$$V_f^2 \simeq \frac{8mv_{ph}F(\omega_p L/v_{ph})}{\pi\epsilon_0\langle v^2\rangle}\left[\frac{\sum_i \int_{v_{ph}}^{\infty} dv\ v\ f_i(v)}{\sum_i f_i(v_{ph})}\right] \tag{55}$$

where

$$v_{ph} \simeq \omega_p/k_L \simeq (\langle v^2\rangle f_p/2\Delta f)^{1/2} \simeq [(3k_B T/2m)(f_p/\Delta f)]^{1/2} \tag{56}$$

and in (55)-(56), $\langle v^2\rangle$ and T (the kinetic temperature) concern the whole velocity distribution. One sees from (55) that the noise at frequency $f = f_p + \Delta f$ is produced by electrons moving faster than v_{ph} given by (56). The detailed shape of the peak is governed by the value of $\omega_p L/v_{ph}$ (determining F given by (10)) and by the electron population f_i that dominates the bracket in (55). If $f(v) \simeq f_i(v)$ for $v \geqslant v_{ph}$, the same population i dominates both the numerator and the denominator of this bracket, which simplifies to

$$[...] \simeq \int_{v_{ph}}^{\infty} dv\ v\ f_i(v)/f_i(v_{ph}) \tag{57}$$

Hence in that case the amplitude and shape of the QTN peak depend only on the shape of the component i of the distribution and not of its relative density.

Consider the case when at speeds $v \gtrsim v_{ph}$, the distribution can be approximated by a hot Kappa halo given by (27) with density n_h and temperature $T_h = (mv_0^2/2k_B)[\kappa/(\kappa - 3/2)]$. With for example $n_h/n = 0.05$, $T_h/T = 10$ and $\kappa = 5$, one can verify that this holds when $\Delta f/f_p \lesssim 0.1$ (when the core is Maxwellian). The bracket in (55) then reduces to

$$[...] \simeq \frac{k_B T_h}{m} \frac{\kappa - 3/2}{\kappa} \left[1 + \frac{3T}{4T_h(\kappa - 3/2)} \frac{f_p}{\Delta f} \right] \tag{58}$$

When $\Delta f/f_p > 3T/[4T_h(\kappa - 3/2)]$, which holds with the above parameters when $\Delta f/f_p > 0.02$, the bracket in (58) reduces to unity in order of magnitude, so that (55) and (58) yield

$$V_f^2 \simeq \frac{8 m v_{ph} F(\omega_p L/v_{ph})}{3\pi\epsilon_0} \frac{T_h}{T} \frac{\kappa - 3/2}{\kappa} \tag{59}$$

An interesting property emerges from (59). In this exterior part of the peak ($0.02 < \Delta f/f_p < 0.1$ with the above parameters), the power is not only independent of the density of the halo, it is also similar for a Kappa halo and a Maxwellian halo ($\kappa \to \infty$), if they have similar most probable speeds ($v_0 = [(\kappa - 3/2) \times T_h/\kappa]^{1/2}$, from (28)). Let us estimate the amplitude of the peak in this frequency range. We have from (56) and (26)

$$\frac{\omega_p L}{v_{ph}} \simeq \frac{L}{L_D} \left(\frac{T_{-2}}{T} \right)^{1/2} \left(\frac{2\Delta f}{3 f_p} \right)^{1/2} \tag{60}$$

For $\Delta f/f_p \simeq 0.05$ (which lies in the range determined above) and $L/L_D < 5$, (60) yields $\omega_p L/v_{ph} < 1$, so that $F(\omega_p L/v_{ph}) \simeq (\omega_p L/v_{ph})^2/24$ and (59) and (56) yield $V_f^2/T^{1/2} \simeq 5 \times 10^{-16}$ for $L/L_D \simeq 5$.

Closer to f_p ($\Delta f/f_p < 0.02$ in our example), the right-hand side term of the bracket in (58) becomes dominant, which means that v_{ph} is such that the electrons producing the noise are in the speed range where the hot kappa distribution (27) behaves as a power law velocity distribution $f(v) \propto v^{-p}$ with $p = 2(\kappa + 1)$. In that case, (58) yields

$$[...] \simeq \frac{3 k_B T}{4 m \kappa} \frac{f_p}{\Delta f} \tag{61}$$

which no longer depends on T_h (nor n_h), and we get from (55), (56), (11), (60) and (61)

$$V_f^2 \simeq \frac{(mk_BT)^{1/2}}{6^{3/2}\pi\epsilon_0\kappa}\frac{T_{-2}}{T}\frac{L^2}{L_D^2}\left(\frac{f_p}{\Delta f}\right)^{1/2} \tag{62}$$

so that the power increases strongly very close to f_p, as $(f_p/\Delta f)^{1/2}$, yielding a peak located at f_p. This contrasts with the behavior for a Maxwellian halo ($\kappa \to \infty$), in which case the bracket (58) equals k_BT_h/m, so that (55) yields

$$V_f^2 \simeq \frac{8mT_hv_{ph}}{3\pi\epsilon_0 T}F(\omega_pL/v_{ph}) \tag{63}$$

Equation (63) shows that when $\Delta f \to 0$ ($v_{ph} \to \infty$), $V_f^2 \to 0$, so that the noise peak is shifted above f_p [*Meyer-Vernet and Perche*, 1989], at the value of Δf for which $v_{ph}F(\omega_pL/v_{ph})$ is maximum.

Let us use these results to determine whether QTN spectroscopy can be used to measure the solar wind super-halo electrons, which have a nearly isotropic power-law velocity distribution at energies exceeding $E_0 \simeq 2$ keV [e.g., *Wang et al.*, 2012]. Using v_{ph} given by (56), we see that these electrons are revealed at frequencies $f_p + \Delta f$ with $\Delta f/f_p < (3/4) \times T_{\rm eV}/E_0 \simeq 4 \times 10^{-3}$ if $T \simeq 10$ eV. Such an observation also requires that the f_p fluctuations produced by turbulent density fluctuations [e.g., *Wang et al.*, 2012] occuring during the measurement of the peak do not broaden it by more than Δf, which imposes a constraint on the time resolution that may be difficult to conciliate with the frequency resolution (because of the Nyquist-Shannon theorem). Using (62) with $\kappa = p/2 - 1$, we obtain for $p = 7$ and $L/L_D = 5$, $V_f^2/T^{1/2} \simeq 10^{-16}(f_p/\Delta f)^{1/2}$. For $\Delta f/f_p \simeq 4 \times 10^{-3}$, this yields $V_f^2/T^{1/2} \simeq 1.4 \times 10^{-15}$ V^{2}Hz^{-1}, i.e. about 4×10^{-13} V^{2}Hz^{-1} for $T \simeq 10^5$

K. Since $(1/\Delta f)\int_{f_p}^{f_p+\Delta f} df[f_p/(f-f_p)]^{1/2} = 2$, a receiver with this frequency resolution should mesure twice this power, i.e. $V_f^2 \simeq 10^{-12}$ V^{2}Hz^{-1}.

It is interesting to note that such a very high noise level, corresponding to QTN produced by super-halo electrons, could be erroneously interpreted instead as due to plasma instabilities.

2.7. Flat-top Distributions

Flat-top distributions are observed in various media, under conditions when all particles are accelerated up to a similar energy, for example via an electrostatic field present in a restricted region. Such velocity distributions have been observed in particular in the Earth's magnetosheath [*Feldman et al.*, 1982], the Earth's magnetotail around magnetic reconnection regions [*Asano et al.*, 2008], and downstream of strong interplanetary shocks [*Fitzenreiter et al.*, 2003].

Compared to Maxwellians or Kappas, for which the bulk of the distribution has a relatively similar shape, flat-top distributions have a large excess of medium energy particles, and the "temperatures" defined in (20)-(22) with $q < 0$ generally exceed the kinetic temperature T_2, contrary to distributions with suprathermal tails. For example, the distribution studied by *Chateau and Meyer-Vernet* [1989], $f(v) \propto [1+(v/v_0)^8]^{-1}$, which can approximate distributions measured in the Earth's magnetosheath, has $T_{-2} = 1.24 \times T$ with $T \equiv T_2 = mv_0^2/3k_B$, so that the Debye length largely exceeds that of a Maxwellian of similar temperature. Since in this case $T_{-1} = 1.11 \times T$, we have $T_{-2}/T_{-1}^{1/2} = 0.95 \times T_{-2}^{1/2}$, so that the temperature deduced from the plateau level using (40) is close to that defining the Debye length. However, since $T_{-2}^2/T_{-1} = 1.37 \times T$ this "temperature" exceeds by nearly 40% the kinetic temperature T revealed by the high-frequency QTN using (46) - a behavior which strongly contrasts with that of a Kappa distribution. Therefore, although the QTN diagnostics cannot reveal the full flat-top shape, it can nevertheless give a strong hint of such a shape.

2.8. Ions

Because of their large mass (small characteristic frequency), ions generally play a minor role in the QTN at frequencies of the order of magnitude of the plasma frequency, except when the Doppler-shift of their fluctuations puts them in this frequency range - a case often encountered in the solar wind. Since Ulysses spin axis was close to the solar direction, the equatorial antennas were oriented approximately perpendicular to the solar wind velocity. The contribution of the solar wind ions to the QTN has been calculated in this case [*Issautier et al.*, 1999] and used to estimate the ions properties [*Issautier et al.*, 1998]. We derive below a few additional properties that may be useful for other missions.

Equations (2), (3) and (13) show that if the drift speed is much larger than the ion average speed, the main contribution to the integral in (13) stems from the values of θ satisfying $\omega \simeq kV\cos\theta$. Hence if the antenna is parallel to the drift speed we deduce by substituting $k\cos\theta = \omega/V$ into (16) that the ion QTN is proportional to the factor $[\sin^2(\omega L/2V)/(\omega L/V)]^2$, which oscillates with frequency and goes to zero at frequencies that are multiples of V/L. Such variations have been observed on WIND/WAVES [*Tong et al.*, 2015].

An important simplification arises when $\omega L_D/V \gg 1$, which holds around the plasma frequency in the solar wind for PSP at 10 solar radii ($\omega_p L_D/V \simeq 20$). In that case, the

QTN contribution due to the ions is given by

$$V^2_{f\text{ions}} \simeq \frac{8m_e V^3 \omega_p^2}{\pi\epsilon_0 L^2 \omega^4} \sin^4(\frac{\omega L}{2V}) \qquad \text{antenna } \parallel \mathbf{V} \qquad (64)$$

$$V^2_{f\text{ions}} \simeq \frac{m_e V^2 \omega_p^2}{\epsilon_0 L \omega^3} \qquad \text{antenna } \perp \mathbf{V} \qquad (65)$$

Comparing with (41), one sees that the ion contribution to the QTN is expected to be negligible whatever the antenna direction for PSP at perihelion.

3. QTN in Real Life

Now that QTN spectroscopy has been admitted in the exclusive club of recognized in situ measurement techniques, it is essential to ensure that it is not used loosey-goosey, under conditions which might lead to incorrect results. We therefore discuss below some constraints of real life in space which are (or are not) compatible with accurate measurements by QTN spectroscopy, and derive some results that may be useful for practical applications.

3.1. Unequal Booms

When the antenna wires are too thin, they can be broken by dust impacts. This happened several times for the WIND/WAVES dipole antennas, which now have arms of unequal length. We consider below an antenna made of two wires of respective lengths L_1 and L_2, aligned along the z axis and longer than the gap between them (we do not consider the effect of a gap since this has been calculated by *Meyer-Vernet and Perche* [1989]).

The Fourier transform of the current distribution becomes

$$J_z(\mathbf{k}) = \frac{1}{k_z^2}\left[\frac{e^{ik_z L_1} - 1}{L_1} + \frac{e^{-ik_z L_2} - 1}{L_2}\right] \qquad (66)$$

Hence with an isotropic velocity distribution, the QTN is obtained by replacing in (9) $F(kL)$ by $G(kL_1, kL_2)$ given by

$$G(kL_1, kL_2) = \frac{1}{4k}\left(\frac{L_1+L_2}{L_1L_2}\right)\{g(kL_1)+g(kL_2)-g[k(L_1+L_2)]\} \tag{67}$$

$$g(x) = \frac{\cos x - 1}{x} + \mathrm{Si(x)} \tag{68}$$

where Si is the sine integral function. In the particular cases of respectively short and long antennas, (67)-(68) yield

$$G(kL_1, kL_2) \simeq \frac{k^2(L_1+L_2)^2}{96} \quad \text{if} \quad kL_1, kL_2 \ll 1 \tag{69}$$

$$G(kL_1, kL_2) \simeq \frac{\pi}{8k}\frac{L_1+L_2}{L_1L_2} \quad \text{if} \quad kL_1, kL_2 \gg 1 \tag{70}$$

Therefore for short antennas, the unequal arms of lengths L_1, L_2 are equivalent to a symmetric antenna made of wires of length the average length, $L_a = (L_1+L_2)/2$, whereas for long antennas, the unequal arms are equivalent to an antenna of length the inverse of the average of the inverse lengths, $L_g = 2L_1L_2/(L_1+L_2)$. In the frequent case when the antenna is short compared to the electromagnetic wavelength c/f, but long with respect to L_D, this property suggests a quick method for determining separately the lengths of the two antenna arms when they have been broken, using both a known radioemission as the galactic noise and the QTN in a known plasma. Indeed in that case, (69) shows that the reception of electromagnetic waves depends on the arithmetic mean L_a, whereas (70) shows that the QTN depends on the geometric mean L_g; this enables one to determine both L_g and L_a, from which one can deduce directly L_1 and L_2. When the booms are not long enough to use the approximation (70), one must use the exact expression (67).

3.2. Fat and/or Biased Antennas

To be adequate for thermal noise spectroscopy, electric antennas must not only be long enough (albeit not too long [*Meyer-Vernet et al.*, 2000]), they must also be thin enough. There are two basic constraints on the radius of electric antennas. First its must be small compared to the Debye length, otherwise the approximation $k_\perp a \ll 1$ in Eq.(8) does not hold true, producing additional resonances - a problem only encountered in dense planetary ionospheres; a further problem arises in that case (see Section 4). The second constraint is due to the shot noise, since fat antennas may collect or emit so many electrons that the corresponding shot noise may exceed the quasi-thermal noise. Since each electron collection or emission from or to the ambient plasma produces a voltage pulse of rise time $\sim (2\pi f_p)^{-1}$ ($\sim (2\pi f_{ph})^{-1}$ for photoelectrons of plasma frequency f_{ph}) and a generally much longer decay time, τ_d, due to the discharge of the antenna, the shot noise has a f^{-2} spectrum for $(2\pi\tau_d)^{-1} < f < f_p$ (the squared Fourier transform of a Heaviside function). In practice, if the electron collection is not much affected by the antenna electric potential Φ (which requires the condition $e|\Phi| \ll k_B T_e$), the shot noise below the plasma frequency at the antenna ports can be approximated by

$$V_{\rm shot}^2 \simeq 2|I_{e0}| \times e/C_a^2\omega^2 \simeq 2 \times 10^{-16}(a/L)[\ln(L_D/a)]^2 T_1^{1/2}(f_p/f)^2 \qquad (71)$$

for $a < L_D < L$ (from Eq.(25) and the formulas by [*Meyer-Vernet and Perche*, 1989]), where $C_a \simeq (i\omega Z_a)^{-1}$ is the dipole antenna capacitance and I_{e0} is the electron current on one antenna arm when $\Phi = 0$. Comparing with the expression (40) of the QTN, (71) yields

$$V_{\rm shot}^2/V_{\rm QTN}^2 \simeq 4.9 \times \tau(a/L)[\ln(L_D/a)]^2(f_p/f)^2 \quad (72)$$

with $\tau = T_1^{1/2}T_{-1}^{1/2}/T_{-2}$, which equals unity for a Maxwellian electron distribution, whereas $\tau \gtrsim 1$ when the distribution has a suprathermal tail; for example, with a Kappa distribution we have $\tau = (\kappa - 1/2)/(\kappa - 1)$. With the parameters listed in Table 1 and $\tau \simeq 1$, (72) yields $V_{\rm shot}^2/V_{\rm QTN}^2 \simeq 0.4 \times (f_p/f)^2$ for SO and $V_{\rm shot}^2/V_{\rm QTN}^2 \simeq 0.14 \times (f_p/f)^2$ for PSP at perihelion. As noted above, these results assume the frequency to be smaller than f_p and to exceed the inverse of the decay time $\tau_d \simeq RC_a$ of the antenna potential pulses produced by electron impacts and emission, so that these pulses are roughly step-like; here R is the low-frequency antenna resistance due to its discharge by photoelectron emission and plasma collection [*Henri et al.*, 2011]; at smaller frequencies the shot noise is smaller by the factor $\omega\tau_d$.

The expression (71) of the shot noise also assumes both that the electron collection is not much affected by the antenna electric potential Φ, and that this potential is the floating potential for which the electron collection current is mainly balanced by the photoelectron emission current or by the ion current if the latter is larger. This may not be the case if the antenna is biased since in that case the change in antenna potential may change significantly the number of elementary charges transferred from and to the antennas, whereas the bias current, I_b, also contributes to the shot noise. Indeed, since each individual charge transfer to the antenna contributes additively to the shot noise, positive and negative current pulses do not cancel out and they all contribute to the fluctuations.

Let us first consider the case when the ambient medium is the solar wind. In this case, the photoelectron current I_{ph0} typically exceeds the plasma electron current I_{e0} by one order of magnitude (here the subscript '0" stands for the currents on an antenna arm when $\Phi = 0$). Hence the antenna potential Φ floats at a few times the photoelectron temperature $T_{ph(\mathrm{eV})}$, in order that the ejected photoelectron current

$$I_{ph} \simeq I_{ph0} \times e^{-\Phi/T_{ph(\mathrm{eV})}} \tag{73}$$

balances the collected electron current

$$I_e \simeq I_{e0} \times (1 + \Phi/T_{e(\mathrm{eV})}) \tag{74}$$

where we have assumed Maxwellian distributions with $\Phi/T_{e(\mathrm{eV})} \ll 1$ since $T_{ph} \ll T_e$ [*Whipple*, 1981]. In that case, the shot noise (71) is increased by the factor $I_e/I_{e0} \simeq (1 + \Phi/T_{e(\mathrm{eV})})$. This result also holds in presence of secondary electron emission I_{sec} since in that case $|I_{sec}| + |I_{ph}| = |I_e|$ (neglecting the smaller ion current). Note that we have neglected the shot noise produced by the photoelectrons returning to the antenna because at frequencies $f < f_p$ the corresponding pulse duration ($\simeq 1/(2\pi f_{ph})$) is much shorter than $1/(2\pi f)$.

If the antenna is biased with a bias current I_b (per antenna arm), the shot noise (71) becomes

$$V_{\mathrm{shot}}^2 \simeq (|I_e| + |I_{ph}| + |I_b|)e/C_a^2\omega^2 \tag{75}$$

since it is proportional to the total number of elementary charges transferred from or to the antenna per time unit, and the contribution of the bias current to the shot noise is estimated by assuming that the corresponding impedance is essentially due to the antenna capacitance. Since $I_b = |I_{ph}| - |I_e|$, we deduce

$$V_{\text{shot}}^2 \simeq 2e \times \text{Max}(|I_{ph}|, |I_e|)/C_a^2\omega^2 \tag{76}$$

Consider the case when, due to the bias, the antenna potential becomes much smaller than both $T_{ph(\text{eV})}$ and $T_{e(\text{eV})}$, so that $|I_{ph}| \simeq |I_{ph0}|$ and $|I_e| \simeq |I_{e0}| \ll |I_{ph}|$. In that case (76) shows that the bias increases the shot noise (71) by the approximate factor $|I_{ph0}/I_{e0}|$, which amounts to about one order of magnitude in the solar wind; such a bias would make the shot noise largely dominant over the QTN for SO and of the same order of magnitude as the QTN for PSP. On the other hand, biasing the antenna in order to increase its positive potential Φ would increase the shot noise by a smaller factor. Note that the above estimates assume the antenna photoelectron current to be given by (73), even at small heliocentric distances because - contrary to the spacecraft PSP [*Ergun et al.*, 2010] - the antennas, whose radius is smaller than the photoelectron Debye length, are not expected to be surrounded by a potential barrier reflecting the emitted photoelectrons.

Consider now dense planetary environments, when the plasma ion current dominates the photoelectron current. In that case, since $|I_{i0}/I_{e0}| \simeq (m_e T_{1i}/m_i T_{1e})^{1/2} \ll 1$, the antenna potential floats to a negative value of order a few times the plasma electron temperature in order to decrease the plasma electron current $I_e \simeq I_{e0} \times e^{-|\Phi|/T_{e(\text{eV})}}$ sufficiently to balance the plasma ion current given by $I_i \simeq I_{i0} \times (1 + |\Phi|/T_{i(\text{eV})})$ for $\Phi/T_{i(\text{eV})} \ll 1$ [*Whipple*, 1981]. In that case, the shot noise (71) is decreased by the factor $I_e/I_{e0} \simeq e^{-|\Phi|/T_{e(\text{eV})}}$.

With a bias current, the shot noise is given by (75)-(76) with $|I_{ph}|$ replaced by $|I_i|$. In that case, if because of the bias, the potential $|\Phi|$ becomes much smaller than both $T_{i(\text{eV})}$

and $T_{e(\mathrm{eV})}$, we have $|I_i| \simeq |I_{i0}|$ and $|I_e| \simeq |I_{e0}| \gg |I_i|$, so that $\mathrm{Max}(|I_i|, |I_e|) \simeq |I_{e0}|$ and the shot noise is thus given by (71). In contrast, a bias making the antenna potential more negative would decrease the shot noise.

3.3. Dusty Plasmas: Quasi-Thermal Noise of Charged Dust Grains

Virtually every plasma contains dust particles [*Shukla and Mamum*, 2002]. They can affect plasma waves in two ways. First, when dust grains impact solid surfaces at high-speed, they are vaporized and partially ionized, as well as the material of the impacted surface; this produces an expanding plasma cloud which affects the ambient electric field, whereas some plasma particles are recollected by the spacecraft or antennas; these processes can be detected by radio receivers and are currently used for dust detection (e.g. *Meyer-Vernet et al.* [2016] and references therein) complementary to dedicated dust detectors (e.g. *Auer* [2001]). Second, since dust grains carry electric charges (e.g. *Mann et al.* [2014]), their motion produces an electric field, which can be detected by the electric antennas. We consider below the latter mechanism, and assume that the concentration of dust grains is small enough that they do not affect the plasma dielectric function [*Verheest*, 1996].

In order to compare this mechanism to impact ionization, consider the charge carried by a dust particle of radius r_d and floating potential Φ_d

$$q \simeq 4\pi\epsilon_0 r_d \Phi_d \tag{77}$$

where Φ_d equals a few times the temperature (in eV) of the particles that govern the grains' charging, i.e., photoelectrons in the solar wind or ambient electrons in dense planetary environments. Beware that (77) no longer holds when the grain's size is smaller than the Landau radius (the distance at which the mutual electrostatic energy of two plasma electrons equals their thermal energy), because of both the grains' polarization and the charge quantization [e.g., *Meyer-Vernet*, 2013].

Comparing q with the charge involved in impact ionization for a grain of mass m_d impacting at speed v_d, $Q \simeq 0.7 m_d v_{d(\mathrm{km/s})}^{3.5}$ [*McBride and McDonnell*, 1999; *Lai et al.*, 2002], we have

$$q/Q \simeq 0.015 \times r_{d(\mu\mathrm{m})}^{-2} v_{d(\mathrm{km/s})}^{-3.5} \Phi_d \tag{78}$$

Equation (78) generally yields $q/Q \ll 1$, except for submicron particles moving slowly, for example nanodust that have not yet been accelerated, such as freshly produced nanodust in the solar wind or nanodust in inner planetary magnetospheres.

Let us now compare the number of dust particles affecting the electric antennas in dipole mode for both mechanisms. The rate of passing-by dust particles affecting the antennas exceeds the impact rate on their surface by the large factor L_D/a, of order of magnitude 10^4 for the cases listed in Table 1 (we do not consider the impacts on the spacecraft, which are generally not efficiently detected in dipole mode). These numbers suggest that the electric noise produced by dust grains passing by the antennas may be worth considering. Such a measurement via a time domain sampler has been discussed by *Meuris et al.* [1996]. We consider below the possibility of such a measurement via a wave receiver, i.e. the quasi-thermal noise produced by dust grains moving around the antennas.

In order to derive order-of-magnitude estimates, we consider a simple case: dust grains of charge q and isotropic velocity distribution $f_d(v)$. From Eqs. (2), (9) and (33), their QTN is given by

$$V_{f\mathrm{d}}^2 = \frac{32q^2}{\epsilon_0^2}\int_0^\infty dk \frac{F(kL)}{k^3|\epsilon_L(\mathbf{k},\omega)|^2}\int_{\omega/k}^\infty dv\ v\ f_d(v) \tag{79}$$

where $F(x)$ is given by (10). We now make the further simplifying assumption that the grains have a similar speed V_d, so that their distribution can be approximated by

$$f_d(v) = n_d\delta(v - V_d)/(4\pi V_d^2) \tag{80}$$

n_d being their number density. Substituting (80) into (79) yields

$$V_{f\mathrm{d}}^2 = \frac{8n_d q^2}{\pi\epsilon_0^2 V_d}\int_{\omega/V_d}^\infty dk \frac{F(kL)}{k^3|\epsilon_L(\mathbf{k},\omega)|^2} \tag{81}$$

Since V_d is much smaller than the electron thermal speed, we can use the approximation (35) of ϵ_L in the integral (81), which reduces to $\epsilon_L \simeq 1$ since $kL_D \gg 1$ in the integration range. This yields the QTN of this dust distribution

$$V_{f\mathrm{d}}^2 = \frac{8n_d q^2 L^2}{\pi\epsilon_0^2 V_d}\int_{\omega L/V_d}^\infty dx \frac{F(x)}{x^3} \tag{82}$$

Using the approximations (11) and (12), we deduce in particular

$$V_{f\mathrm{d}}^2 = \frac{2n_d q^2 V_d^2}{3\epsilon_0^2 L\omega^3} \qquad \text{for } \omega L/V_d \gg 1 \tag{83}$$

$$V_{f\mathrm{d}}^2 = \frac{n_d q^2 L^2}{3\pi\epsilon_0^2 V_d}\ln(V_d/\omega L) \quad \text{for } \omega L/V_d \ll 1 \tag{84}$$

For example, a concentration $n_d \simeq 10^3$ cm^{-3} of nanodust of radius a few nanometers moving at $V_d \simeq 15$ km/s relative to the Cassini spacecraft in Enceladus' plume [*Hill et al.*, 2012] should produce from (83) a QTN power of order of magnitude $V_{f\mathrm{d}}^2 \simeq 10^{-10}$ V^{2}Hz^{-1} near 1 kHz. This level is expected to largely exceed the shot noise due to plasma particle impacts because of the strong electron depletion [*Hill et al.*, 2012].

4. Concluding Remarks

We have provided a number of new tools for implementing QTN spectroscopy in space plasmas, which are generally not in thermal equilibrium and are sometimes dusty, inboard various missions. In particular, we give an exact generic expression of the "cold" electron temperature and of its measurement via the QTN plateau (36); we also give a generic analytical approximation (40) of this plateau valid for practical antenna lengths in space, and provide an application for PSP at perihelion. The QTN plateau level is all the more generic, given that we have proven that it still holds in presence of a magnetic field. We also give new analytical approximations of the QTN peak shape and level in several practical cases, and study the conditions in which the solar wind super halo might be measured by this technique. Concerning flat-top distributions, we suggest a simple method to infer them by comparing the low and high frequency QTN levels. Finally, we give new analytical approximations for the QTN due to ions in the solar wind, and show that this component is expected to be negligible for PSP at perihelion.

In order to adapt the method to various practical situations in space, we have considered antennas made of two wires of different lengths, as occurs on WIND after damaging of the antennas by dust impacts, and suggest a new method for determining separately the lengths of the dipole arms. We also consider fat and/or biased antennas, showing that biasing might considerably increase the shot noise in the solar wind, possibly spoiling QTN measurements. Finally, we have estimated the QTN produced by the motion of dust grains near the antennas, yielding a new method to measure grains when their speed is not high enough for producing significant impact ionization. This result may be applied for detecting nanodust in the Enceladus plume, where the plasma shot noise is expected to be small because of the strong electron depletion (due to capture of most plasma electrons by the grains) [*Hill et al.*, 2012], so that the dust QTN noise may dominate the spectrum at low frequencies.

Further extensions will be necessary in the near future to implement QTN spectroscopy on the cubesat projects [e.g., *Swartwout*, 2013; *Saint-Hilaire et al.*, 2014] in the Earth's ionosphere. Even though collisions are negligible at normal cubesat altitudes, they should be taken into account at lower altitudes (the E region); such an extension has already been considered [*Meyer and Vernet*, 1975; *Martinovic et al.*, 2017]. Another simple extension which has already been considered [*Meyer-Vernet and Perche*, 1989] is the accounting of the gap between antenna arms due to the presence of the satellite if its diameter is not small compared to the antenna length. A much more difficult problem is that the negative floating potential of the antenna, of modulus greater than the electron temperature (in eV) will produce a sheath depleted of electrons around the antenna, of width several Debye lengths [*Laframboise*, 1966], because the antenna radius will not be small compared to the Debye length (typically a fraction of centimeter). A detailed study of the impedance of a wire dipole antenna in the Earth's ionosphere has shown that this effect can be approximately taken into account at frequencies $f > f_p$ by making a simple extension of the theory [*Meyer and Vernet*, 1975], putting in series the impedance of an antenna of radius comparable to that of the sheath, G (the antenna radius plus a few Debye lengths) and that corresponding to the capacitance of a vacuum sheath $(\pi\epsilon_0 L/\ln(G/a))$. However, at frequencies $f < f_p$, a new effect arises: the local plasma frequency in some region of the depleted sheath equals the frequency f, yielding resonances with associated non-collisional losses [*Meyer-Vernet et al.*, 1977]. This effect produces a strong increase of the antenna resistance [*Meyer-Vernet et al.*, 1978] (and therefore of the QTN) and requires a major extension of the theory to be accounted for.

Other extensions will be necessary for applications in the inner solar system. The electron distribution close to the Sun is expected to have significant anisotropies, in particular due to the suprathermal electrons focused along the magnetic field - the so-called strahl [e.g., *Marsch*, 2006]. The effects of electron temperature anisotropies on the QTN at low and high frequencies have been estimated by *Meyer-Vernet* [1994], whereas the effects of the electron bulk speed on the QTN cut-off at the plasma frequency have been considered by *Issautier et al.* [1999]. However, the effects of drift or focusing of suprathermal electrons, which is an important topic, has not yet been studied. And since Nature always turns out to be subtler than we imagine, the future diagnostics will most probably require further and as yet unanticipated extensions of the QTN theory.

Acknowledgments. The authors thank the CNES and the CNRS for support on the Ulysses/URAP, Wind/WAVES and Cassini/RPWS HF projects, and Mélody Pallu and Mathieu Vachey for their help on data processing for Figure 6. The data presented in this paper can be accessed by contacting the authors.

References

Abramowitz, M. and I. A. Stegun (1965), *Handbook of mathematical functions*, Dover, New York.

Alexandrov, A. F., L. S. Bogdankevich and A. A. Rukhadze (1984), *Principles of plasma electrodynamics*, Springer, Berlin, p. 114.

Asano, Y. et al. (2008) Electron flat-top distributions around the magnetic reconnection region, *J. Geophys. Res.*, *113*, A01207, DOI: 10.1029/2007JA012461.

Auer, S. (2001) Instrumentation, in *Interplanetary Dust*, ed. E. Grün, B. A. S. Gustafson, S. Dermott and H. Fechtig (Heidelberg:Springer), 385-444.

Bale, S. D. et al. (2016), The FIELDS instrument suite for Solar Probe Plus, *Space Sci. Rev.*, DOI: 10.1007/s11214-016-0244-5.

Chateau, Y. F., N. Meyer-Vernet (1989) Electrostatic Noise in Non-Maxwellian Plasmas: "Flat-Top" Distribution Function, *J. Geophys. Res.*, *94*, 15,407-15,414.

Chateau, Y. F., N. Meyer-Vernet (1991) Electrostatic noise in non-Maxwellian plasmas: Generic properties and "kappa" distributions, *J. Geophys. Res.*, *96*, 5825-5836.

Couturier, P., S. Hoang, N. Meyer-Vernet and J.-L. Steinberg (1981) Quasi-thermal noise in a stable plasma at rest: theory and observations from ISEE 3, *J. Geophys. Res.*, *86*, 11,127-11,138.

Dudík et al. (2017), Non-equilibrium processes in the solar corona, transition region, flares, and solar wind, *Solar Physics*, *xx*, xx.

Ergun, R. E. et al. (2010), Spacecraft charging and ion wake formation in the near-Sun environment, *Phys. of Plasmas*, *17*, 072903, doi:10.1063/1.3457484.

Fahr, H. J., M. Heyl (2016) Debye screening under non-equilibrium plasma conditions, *Astron. Astrophys.*, *589*, A85.

Fejer, J. A., J. R. Kan (1969) Noise spectrum received by an antenna in a plasma, *Radio Sci.*, *4*, 721-728.

Feldman, W. C. et al. (1982) Electron heating within the Earth's bow shock, *Phys. Rev. Lett.*, *49*, 199.

Fitzenreiter, R. J., Ogilvie, K., W., Bale, S. D., Vinãs, A. F. (2003) Modification of the solar wind electron velocity distribution at interplanetary shocks, *J. Geophys. Res.*, *108*, 1415-1979, DOI: 10.1029/2003JA009865.

Garrett, H. B. (1981), The charging of spacecraft surfaces, *Rev. Geophys. Space Phys.*, *19*, 577-616.

Gurnett, D. A. et al. (2004), The Cassini radio and plasma wave investigation, *Space Sci. Rev.*, *114*, 395-463.

Henri, P. et al. (2011), Observations of Langmuir ponderomotive effects using the Solar TErrestrial RElations Observatory spacecraft as a density probe, *Physics of Plasmas*, *18*, 082308.

Hill, T. W. et al. (2012), Charged nanograins in the Enceladus plume, *J. Geophys. Res.*, *117*, A05209.

Hoang, S., J.-L. Steinberg, G. Epstein, P. Tilloles, J. Fainberg, R. G. Stone (1980), The low-frequency continuum as observed in the solar wind from ISEE 3 - Thermal electrostatic noise, *J. Geophys. Res.*, *85*, 3419-3430.

Hoang, S. et al. (1992), Solar wind thermal electrons in the ecliptic plane between 1 and 4 AU - Preliminary results from the ULYSSES radio receiver, *Geophys. Res. Lett.*, *19*, 1295-1298.

Issautier, K., N. Meyer-Vernet, M. Moncuquet, S. Hoang (1998) Solar wind radial and latitudinal structure of electron density and core temperature from Ulysses thermal noise spectroscopy, *J. Geophys. Res.*, *103*, 1969-1979.

Issautier, K., N. Meyer-Vernet, M. Moncuquet, S. Hoang, D. J. McComas (1999) Quasi-thermal noise in a drifting plasma: Theory and application to solar wind diagnostic on

Ulysses, *J. Geophys. Res.*, *104*, 6691-6704.

Issautier, K., R. M. Skoug, J. T. Gosling, S. P. Gary, D. J. McComas (2001) Solar wind plasma parameters on Ulysses: Detailed comparison between the URAP and SWOOPS experiments, *J. Geophys. Res.*, *106*, 15665-15676.

Issautier, K., C. Perche, S. Hoang, C. Lacombe, M. Maksimovic, J.–L. Bougeret, S. Salem (2005) Solar wind electron density and temperature over solar cycle 23: Thermal noise measurements on Wind, *Adv. Space Res.*, *35*, 2141-2146.

Issautier, K., G. Le Chat, N. Meyer-Vernet, M. Moncuquet, S. Hoang, R. J. MacDowall, D. J. McComas (2008) Electron properties of high-speed solar wind from polar coronal holes obtained by Ulysses thermal noise spectroscopy: Not so dense, not so hot, *Geophys. Res. Lett.*, *35*, CiteID L19101.

Kawasaki, K., S. Inoue, E. Ewang, K. Toyoda, M. Cho (2016), Measurement of electron emission yield by electrons and photons for space aged material, in *Proceed. 14th Spacecraft Charging Technology Conf.*, eds. Hilgers et al., ESA/ESTEC, Noordwijk, NL.

Knoll, R., G. Epstein, S. Hoang, G. Huntzinger, J. L. Steinberg, J. Fainberg, F. Grena, R. G. Stone, S. R. Mosier (1978) The 3-dimensional radio mapping experiment /SBH/ on ISEE-C, *IEEE Trans.*, *GE-16*, 199-204.

Laframboise, J. G. (1966) Theory of spherical and cylindrical Langmuir probes in a collisionless Maxwellian plasma at rest, *Report 100*, Institute of Aerospace Studies, University of Toronto, Canada.

Lai, S. T., E. Murad, W. J. McNeil (2002) Hazards of hypervelocity impacts on spacecraft, *J. Spacecraft Rockets 39* 106–114.

Le Chat, G., K. Issautier, N. Meyer-Vernet, I. Zouganelis, M. Maksimovic, M. Moncuquet (2009) Quasi-thermal noise in space plasma: "kappa" distributions, *Physics of Plasmas*, *16*, 102903-102903-6.

Le Chat, G., K. Issautier, N. Meyer-Vernet, S. Hoang (2011) Large-Scale Variation of SolarWind Electron Properties from Quasi-Thermal Noise Spectroscopy: Ulysses Measurements, *Solar Phys.*, *271*, 141–148.

Lund, E. J., J. LaBelle, R. A. Treuman (1994) On quasi-thermal fluctuations near the plasma frequency in the outer plasmasphere: A case study, *J. Geophys. Res.*, *99*, 23,651-23,660.

Maksimovic, M., S. Hoang, N. Meyer-Vernet, M. Moncuquet, J.-L. Bougeret, J. L Phillips and P. Canu (1995) Solar wind electron parameters from quasithermal noise spectroscopy and comparison with other measurements on Ulysses, *J. Geophys. Res.*, *100*, 19881–19891.

Maksimovic, M., K. Issautier, N. Meyer-Vernet, C. Perche, M. Moncuquet, I. Zouganelis, S. D. Bale, N. Vilmer, J.-L. Bougeret (2005), Solar wind electron temperature and density measurements on the Solar Orbiter with thermal noise spectroscopy, *Adv. Space Res.*, *36*, 1471-1473.

Mann, I., N. Meyer-Vernet, A. Czechowski (2014), Dust in the planetary system: Dust interactions in space plasmas of the solar system, *Physics Reports*, *536*, 1-39.

Martinovic, M. M., A. Zaslavsky, M. Maksimovic, S. Segan (2017) Electrostatic thermal noise in a weakly ionized collisional plasma, *Radio Sci., 52*, 70-77.

Marsch, E., (2006), Kinetic physics of the solar corona and solar wind, *Living Rev. Solar Phys., 3*, 1.

McBride, N. and J. A. M. McDonnell, (1999), Meteoroid impacts on spacecraft: Sporadics, streams, and the 1999 Leonids, *Planet. Space Sci. 47*, 1005–1013.

Meuris, P., N. Meyer-Vernet and J. F. Lemaire (1996) The detection of dust grains by a wire dipole antenna: the radio dust analyzer, *J. Geophys. Res., 101*, 24,471-24,477.

Meyer, P., N. Vernet (1974) The impedance of a short antenna in a warm magnetoplasma, *Radio Science, 9*, 409416.

Meyer, P., N. Vernet (1975) The impedance of a dipole antenna in the ionosphere, 2, Comparison with theory, *Radio Science, 10*, 529536.

Meyer-Vernet, N., P. Meyer, C. Perche (1977) Noncollisional losses in an inhomogeneous plasma, *Phys. Fluids, 20*, 536-537.

Meyer-Vernet, N., P. Meyer, C. Perche (1978) Losses due to the inhomogeneous sheath surrounding an antenna in a plasma, *Radio Science, 13*, 69-73.

Meyer-Vernet, N. (1979) On natural noises detected by antennas in plasmas, *J. Geophys. Res.*, *84*, 5373–5377.

Meyer-Vernet, N. et al. (1986a), Plasma diagnosis from thermal noise and limits on dust flux or mass in Comet Giacobini-Zinner, *Science*, *232*, 370374.

Meyer-Vernet, N. et al. (1986b), Physical parameters for hot and cold electron populations in Comet Giacobini-Zinner with the ICE radio experiment, *Geophys. Res. Lett.*, *13*, 279-282.

Meyer-Vernet, N. and C. Perche (1989) Toolkit for antennae and thermal noise near the plasma frequency, *J. Geophys. Res.*, *94*, 2405-2415.

Meyer-Vernet, N., S. Hoang, M. Moncuquet (1993) Bernstein waves in the Io plasma torus: A novel kind of electron temperature sensor, *J. Geophys. Res.*, *98*, 21,163-21,176.

Meyer-Vernet, N. (1993), Aspects of Debye shielding, *Am. J. Phys.*, *61*, 249-257.

Meyer-Vernet, N. (1994) On the thermal noise" temperature"in an anisotropic plasma, *Geophys. Res. Lett.*, *21*, 397–400.

Meyer-Vernet, N., S. Hoang, K. Issautier, M. Maksimovic, R. Manning, M. Moncuquet, R. Stone (1998), Measuring plasma parameters with thermal noise spectroscopy, in *Measurement techniques in space plasmas: fields, Geophys. Monograph Ser.,* vol. 103, edited by R. Pfaff et al., AGU, Washington DC., pp. 205-210.

Meyer-Vernet, N., S. Hoang, K. Issautier, M. Maksimovic, M. Moncuquet, G. Marcos (2000), Plasma thermal noise: the long wavelength radio limit, in *Radioastronomy at long wavelengths, Geophys. Monograph Ser.,* vol. 119, edited by R. G. Stone et al., AGU, Washington DC., pp. 67-74.

Meyer-Vernet, N. (2001) Large scale structure of planetary environments: the importance of not being Maxwellian, *Planet. Space Sci.*, *49*, 247-260.

Meyer-Vernet (2013), On the charge of nanograins in cold environments and Enceladus dust, *Icarus, 226*, 583-590.

Meyer-Vernet, N., M. Moncuquet, K. Issautier, and P. Schippers (2016), Frequency range of dust detection in space with radio and plasma wave receivers: Theory and application to interplanetary nanodust impacts on Cassini, *J. Geophys. Res. Space Physics, 121* doi:10.1002/2016JA023081.

Moncuquet, M., N. Meyer-Vernet, S. Hoang (1995), Dispersion of electrostatic waves in the Io plasma torus and derived electron temperature, *J. Geophys. Res.*, *100*, 21697-21708.

Moncuquet, M., N. Meyer-Vernet, S. Hoang, R. J. Forsyth, P. Canu (1997), Detection of Bernstein wave forbidden bands in the Jovian magnetosphere: A new way to measure the electron density, *J. Geophys. Res.*, *102*, 2373-2380.

Moncuquet, M., A. Lecacheux, N. Meyer-Vernet, B. Cecconi, W. S. Kurth (2005), Quasi thermal noise spectroscopy in the inner magnetosphere of Saturn with Cassini/RPWS: Electron temperatures and density, *Geophys. Res. Lett.*, *32*, CiteID L20S02.

Moncuquet, M. et al. (2006a), The radio waves and thermal electrostatic noise spectroscopy (SORBET) experiment on BEPICOLOMBO/MMO/PWI: Scientific objectives and performance, *Adv. Space Res.*, *38*, 680-685.

M. Moncuquet, N. Meyer-Vernet, A. Lecacheux, B. Cecconi, and W. S. Kurth (2006b), Quasi Thermal Noise in Bernstein Waves at Saturn. In H. O. Rucker, W. Kurth, and G. Mann, editors, Planetary Radio Emissions VI, p. 93.

Nicholls, D. C., M. A. Dopita, R. S. Sutherland (2012), Resolving the electron temperature discrepancies in HII regions and planetary nebulae: κ-distributed electrons, *Astrophys. J.*, *752*, 148.

Nyquist, H. (1928), Thermal agitation of electric charge in conductors, *Phys. Rev.*, *23*, 110.

Ockham, W. of (1324), *Summa Totius Logicae*, *i. 12.*

Rostoker, N. (1961), Fluctuations of a plasma, *Nucl. Fusion*, *1*, 101-120.

Saint-Hilaire, P. et al. (2014), The Cubesat Radio Experiment (CURE) and Beyond: Cubesat-based Low Frequency Radio Interferometry, *AGU Fall meeting*, abstract SH53B-4231.

Salem, C., J.-M. Bosqued, D. E. Larson, A. Mangeney, M. Maksimovic, C. Perche, R. P. Lin, J.-L. Bougeret (2001), Determination of accurate solar wind electron parameters using particle detectors and radio wave receivers, *J. Geophys. Res.*, *106*, 21701-21717.

Schiff, M., L. (1970), Impedance of a short dipole antenna in a warm isotropic plasma, *Radio Sci.+*, *5*, 1489-1496.

Schippers, P., M. Moncuquet, N. Meyer-Vernet, A. Lecacheux (2013), Core electron temperature and density in the innermost Saturn's magnetosphere from HF power spectra analysis on Cassini, *J. Geophys. Res.*, *118*, 7170-7180.

Scudder, J., S. Olbert (1979), A theory of local and global processes which affect solar wind electrons: The origin of typical 1 AU velocity distribution functions – Steady state theory, *J. Geophys. Res.*, *84*, 2755.

Scudder, J. D., H. Karimabadi (2013), Ubiquitous non-thermals in astrophysical plasmas: Restating the difficulty of maintaining Maxwellians, *Astrophys. J.*, *770*, 26.

Sentman, D. D. (1982), Thermal fluctuations and the diffuse electrostatic emissions, *J. Geophys. Res.*, *87*, 1455-1472.

Shukla, P. K. and A. A. Mamun (2002) Introduction to dusty plasma physics, IOP Publishing Ltd, Bristol.

Sitenko, A. G. (1967) Electromagnetic fluctuations in plasmas, Academic Press, San Diego, USA.

Swartwout, M. (2013), The First One Hundred CubeSats: A Statistical Look, *JoSS*, *2*, 213-233.

Tong, Y., M. Pulupa, C. S. Salem, S. D. Bale (2015), Investigating WIND quasi-thermal noise spectra between the ion and the electron plasma frequency, *AGU Fall Meeting 2015*.

Vasyliunas, V. M. (1968), A survey of low-energy electrons in the evening sector of the magnetosphere with Ogo 1 and Ogo 3, *J. Geophys. Res.*, *73*, 2839-2885.

Verheest, F. (1996), Waves and instabilities in dusty space plasmas, *Space Sci. Rev.*, *77*, 267-302.

Wang, L. et al. (2012), Quiet-time interplanetary $\simeq 2 - 20$ keV superhalo electrons at solar minimum, *Astrophys. J. Lett.*, *753*, L23.

Whipple, E. C. (1981), Potentials of surfaces in space, *Rep. Prog. Phys.*, *44*, 1197–1250.

Yoon, P. H. (2014), Electron kappa distribution and quasi-thermal noise, *J. Geophys. Res.*, *119*, 7074–7087.

Yoon, P. H., S. Kim, G. S. Choe, Y.-J. Moon (2016), Revised model of the steady-state solar wind halo electron velocity distribution function, *Astrophys. J.*, *826*, 204.

Yoon, P. H., J. Hwang, D. K. Shin (2017), Upper hybrid waves and energetic electrons in the radiation belt, *J. Geophys. Res.*, *122*, 5365-5376.

Zouganelis, I., Maksimovic, M., Meyer-Vernet, N., Issautier, K., Moncuquet, M., Bale, S. D. (2007), Implemention of the thermal noise spectroscopy on Solar Orbiter, in *Proceed. 2nd Solar Orbiter workshop*, ESA-SP 641, eds. Marsch, E., Tsinganos, K., Marsden, R., Conroy, L., Noordwijk, Netherlands.

Zouganelis, I. (2008), Measuring suprathermal electron parameters in space plasmas: Implementation of the quasi-thermal noise spectroscopy with kappa distributions using in situ Ulysses/URAP radio measurements in the solar wind, *J. Geophys. Res., 113*, A08111, doi:10.1029/2007JA012979.

Zouganelis, I. et al. (2010), Measurements of stray antenna capacitance in the STEREO/WAVES instrument: Comparison of the measured voltage spectrum with an antenna electron shot noise model, *Radio Sci., 45*, RS1005, doi:10.1029/2009RS004194.

Table 1. Properties of wire dipole antennas (length L of each element, radius a, and dipole stray capacitance[b]) used for QTN on ISEE 3-ICE/3D Radio Mapping, Ulysses/URAP[a] , WIND/WAVES, Cassini/RPWS, MMO-BepiColombo/PWI-WPT, Solar Orbiter (SO)/RPW and Parker Solar Probe (PSP)/FIELDS, and average Debye length in the solar wind at respectively 1 AU (ISEE 3, Ulysses, Wind), 0.3 AU (representative for Bepi-Colombo and SO), 10 R_s (closest heliocentric distance of PSP), and in Saturn's magnetosphere at Enceladus' orbit (explored by Cassini).

Property	ISEE 3	Ulysses	WIND	Cassini	BepiColombo	SO	PSP
L (m)	45	35	50[c]	10	15	6.5	2
a (mm)	0.2	1.1	0.2	14.3	0.21	14.2	1.59
C_b (pF)	45	57	20	55	50?[b]	?[b]	35[b]
L_D (m)	10	10	10	1	5	5	0.8

[a] For Ulysses antennas (tapes of length L, width 5 mm and thickness 0.04 mm), the radius is that of the cylinder having the same capacitance.

[b] The base capacitance can be measured accurately only after the antennas have been extended on the spacecraft in space.

[c] The length indicated holds at the times when Figs 6 and 7 were acquired, i.e. before the antenna wires were broken by dust impacts.

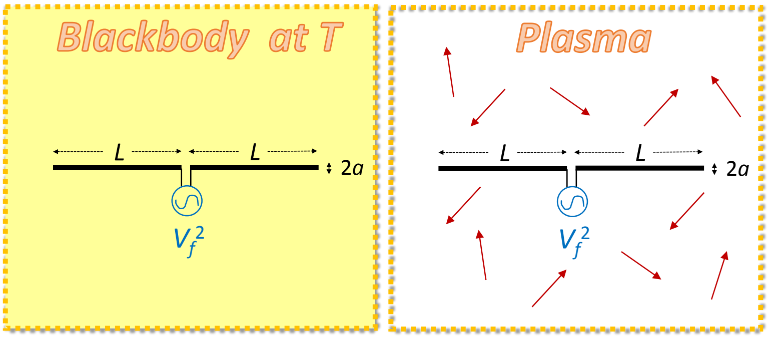

Figure 1. Simple electric antenna (two aligned wires of length L and radius a) immersed in blackbody radiation (left) and in a plasma (right). When $L_D \ll L \ll \lambda = c/f$ (L_D is the plasma Debye length, c the speed of lignt and f the frequency), the antenna resistances are respectively $R_{EM} = 2\pi f^2 L^2/(3\epsilon_0 c^3)$ (left) and $R_P \simeq (2/\pi)^{-1/2}(8\pi\epsilon_0 f_p L)^{-1}$ just below the plasma frequency f_p peak, and $R_P \simeq f_p^2(4\pi\epsilon_0 f^3 L)^{-1}$ for $f \gg f_p$ (right).

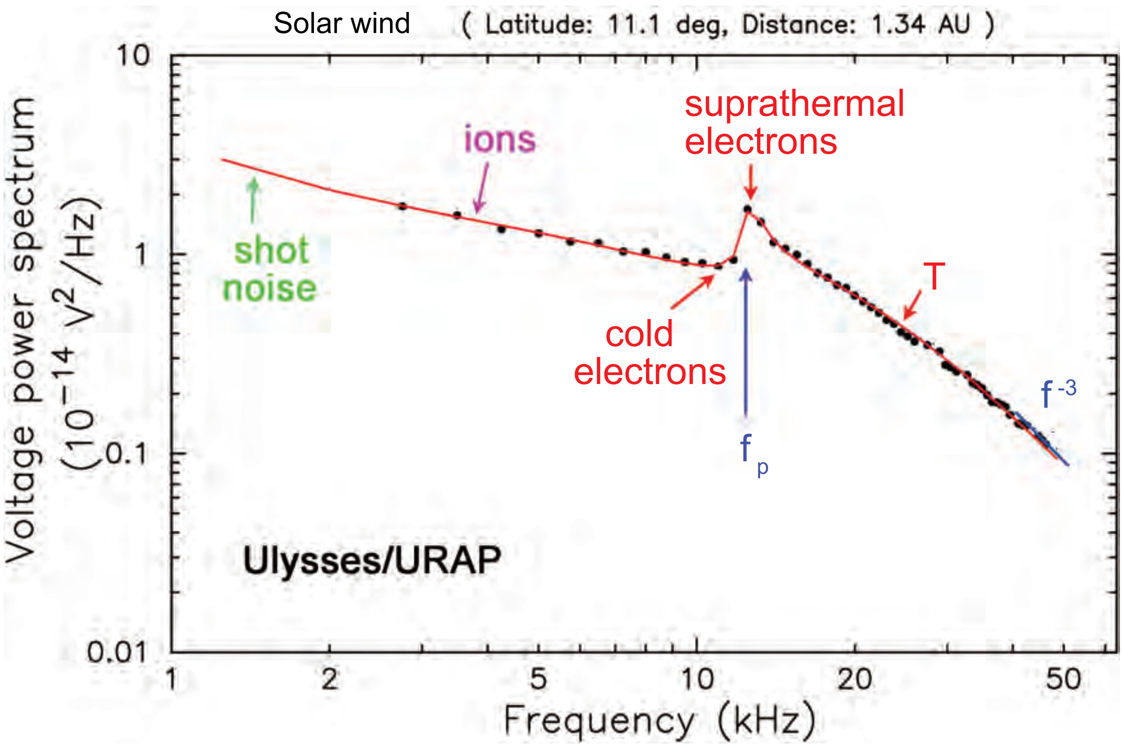

Figure 2. Example of QTN spectrum (V_r^2, measured at the receiver's ports) with a wire dipole antenna in a weakly magnetized plasma (Ulysses/URAP data in the solar wind). The main plasma parameters that can be deduced are indicated. Fitted electron parameters, assuming an electron velocity distribution made of a sum of a cold and a hot maxwellian are: $n = 1.8 \times 10^6$ m^{-3}, $T_c = 1.3 \times 10^5$ K, $T_h/T_c = 8$, $n_h/n_c = 0.04$ (with an accuracy of 1% on n and 7 % on T). Note that for a quick diagnostics, one can deduce the total electron density from the f_p peak, the cold electron temperature from (41) and the kinetic electron temperature from (46), using V_f^2 caculated via (44) with C_a from (43) and (47) at respectively low and high frequencies.

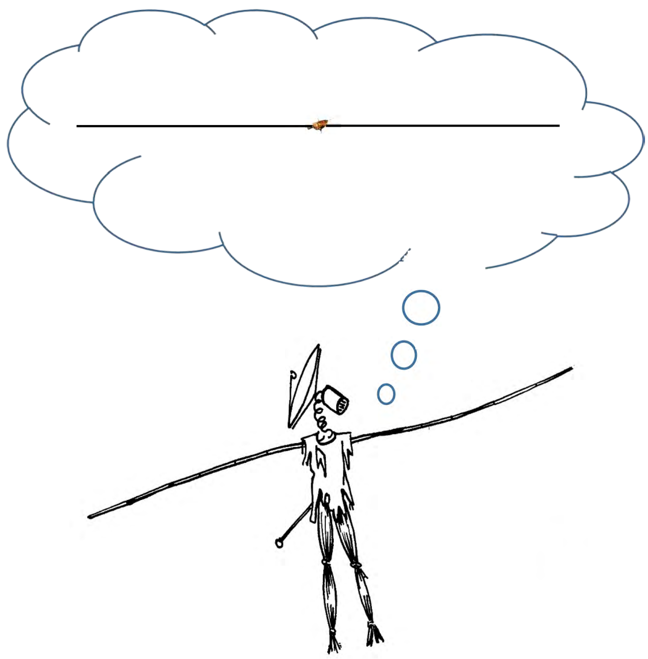

Figure 3. Unfortunately, the strawman payload of the space agencies (bottom) is different from the ideal case for QTN spectroscopy (top), when the spacecraft size is much smaller than the antenna length and the antennas are thin, symmetrical and unbiased - as for ISEE 3 and Ulysses (shown to scale between the antenna wires). Drawing by François Meyer.

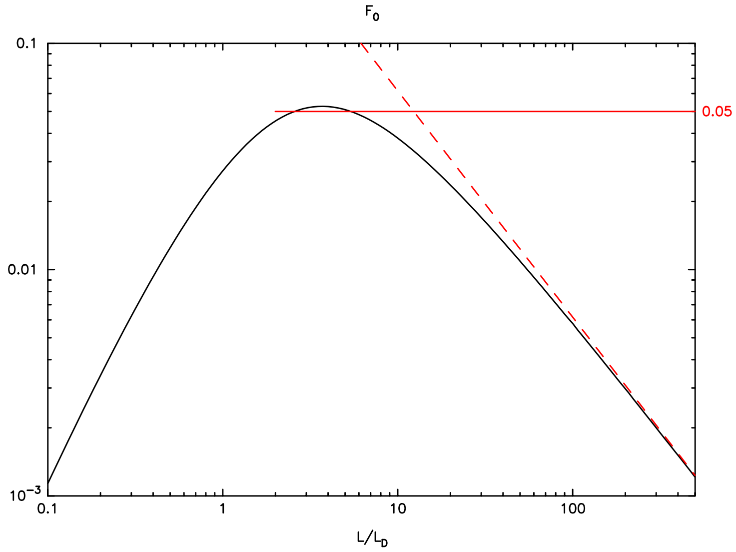

Figure 4. Function $F_0(L/L_D)$ given by (37). Multiplying F_0 by the factor $2^{7/2}(mk_B)^{1/2}/(\pi^{3/2}\epsilon_0) \simeq 8.14 \times 10^{-16}$ yields the QTN plateau V_f^2 normalized to $[T_{-2}/T_{-1}^{1/2}]$, close to the square root of the "cold" temperature (in $\mathrm{V^2Hz^{-1}K^{-1/2}}$) (see Eq.(36)). The dashed red line shows the approximation (38) (valid for very long antennas); the solid red line shows the approximation $F_0 \simeq 0.05$ (valid for intermediate lengths).

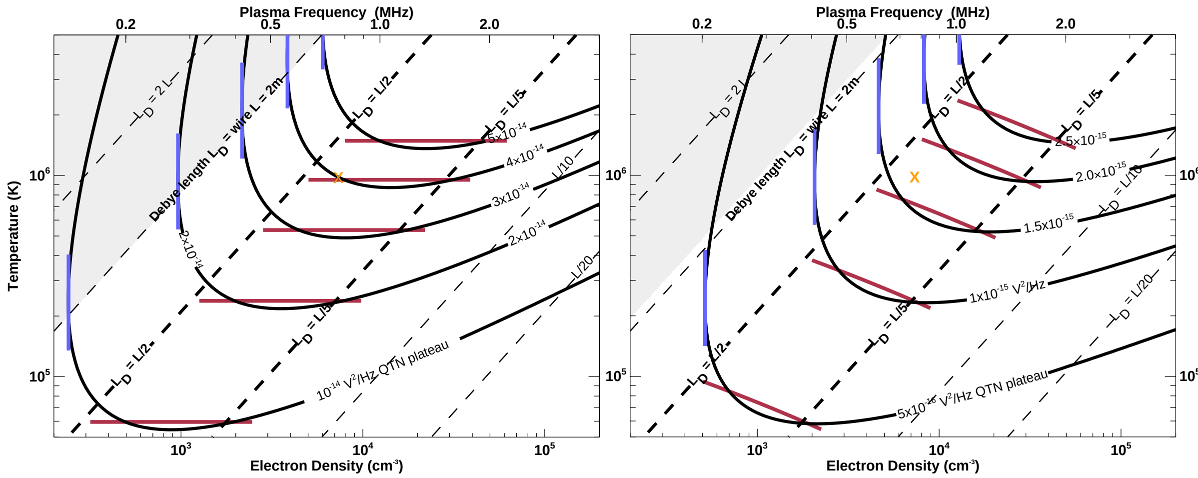

Figure 5. QTN plateau level in $\mathrm{V^2Hz^{-1}}$ with the wire dipole antenna of PSP/FIELDS ($L = 2$ m) in a density/temperature plane, with the approximation (40) superimposed as red bars. The power is calculated at both the antenna ports (left, from (36)) and the receiver ports (right, deduced via (7)). The variation in antenna capacitance (43) with L_D makes V_r^2/V_f^2 vary with the electron density, so that the horizontal lines (left) become inclined (right). The orange cross sketches the density and temperature expected for PSP near perihelion. The range $L/L_D < 1$, in which QTN spectroscopy become ineffective is shown in grey; the blue vertical lines show the regions in which the QTN plateau level becomes weakly dependent of temperature, making this derivation difficult.

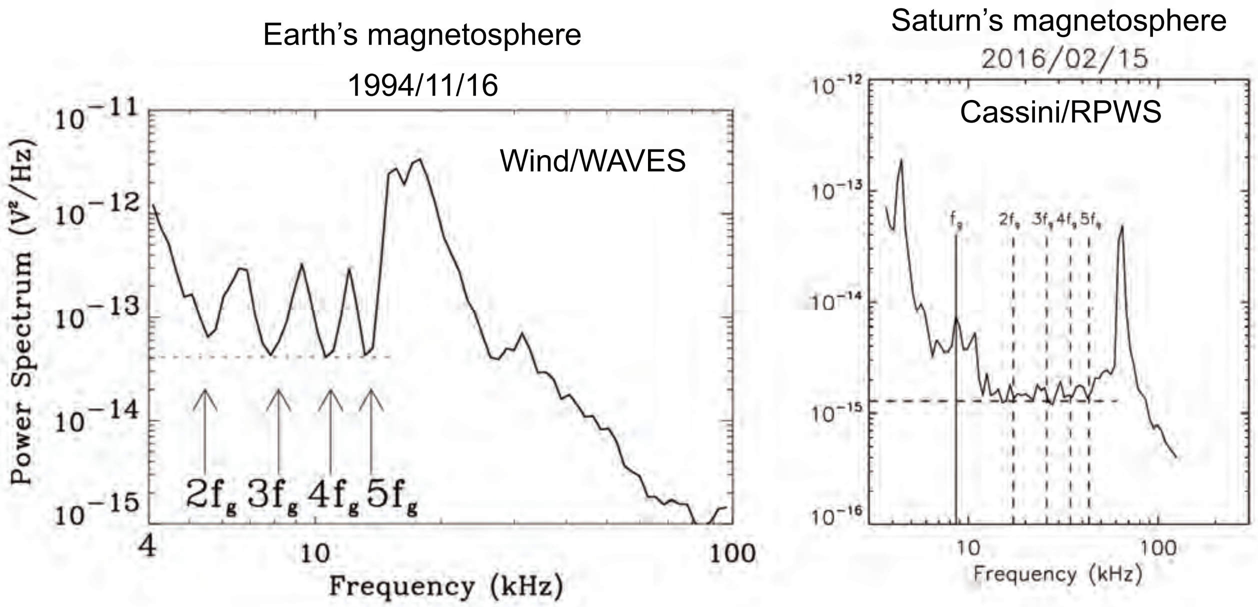

Figure 6. Two examples of quasi-thermal noise spectra (V_r^2, measured at the receiver ports) in magnetized plasmas, showing a plateau of minima (dashed horizontal line) at the gyroharmonics nf_g. Left-hand side: Wind/WAVES data in the Earth's magnetosphere at 8 Earth's radii. Right-hand side: Cassini/RPWS data in Saturn's magnetosphere at 4 Saturn's radii.

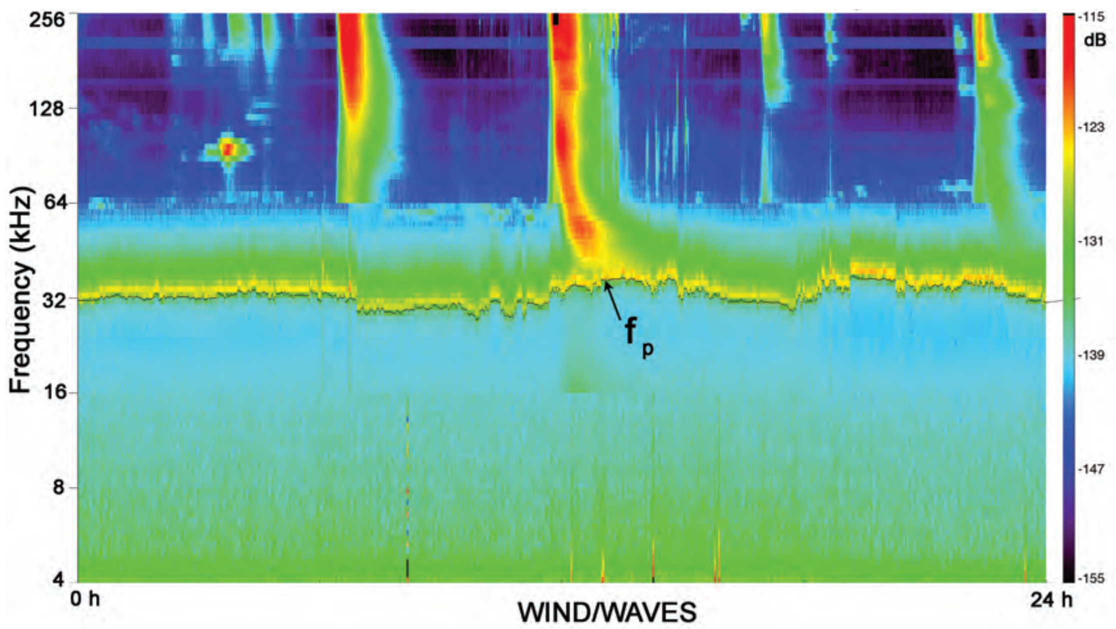

Figure 7. Radio spectrogram from WIND/WAVES acquired on 5 November 1997 in the solar wind, showing solar radioemissions perturbing the plasma QTN above the plasma frequency, whereas the f_p line and QTN plateau are not perturbed. The data are plotted as frequency versus time, with the relative intensity coded as indicated in the color bar.